

Graph Embeddings via Tensor Products and Approximately Orthonormal Codes

Frank Qiu *

Abstract

We analyze a method for embedding graphs as vectors in a structure-preserving manner, showcasing its rich representational capacity and establishing some of its theoretical properties. Our procedure falls under the bind-and-sum approach, and we show that the tensor product is the most general binding operation that respects the superposition principle. We also establish some precise results characterizing the behavior of our method, and we show that our use of spherical codes achieves a packing upper bound. We establish a link to adjacency matrices, showing that our method is, in some sense, a compression of adjacency matrices with applications towards sparse graph representations.

*Statistics Department; University of California, Berkeley

1 Introduction

Graphs are an intuitive way to represent relational information and come up in many applications. However, they are discrete objects, and the wealth of techniques developed for continuous-valued data cannot be easily applied to them. One way to bridge this gap is to embed graph as vectors in a structure-preserving manner, and we analyze a graph embedding method that takes the bind-and-sum approach. Bind-and-sum methods seek to represent a graph’s edgeset through a three-step process:

1. Encode each vertex as a vector
2. Encode each edge by binding the vertex codes of its start and end vertices.
3. Represent the edgeset as a superposition, or sum, of its edge encodings.

We study the tensor-spherical embedding, which uses the tensor product as the binding operation and random spherical vectors as the vertex code. This paper can be roughly divided into two halves.

In the first half, we focus on properties of the tensor-spherical embedding, establishing its rich representational capacity as well as individually analyzing the tensor product and spherical codes. In particular, we show that the tensor product is the most general binding operation and give a derivation from the superposition principle, and we also give a precise characterization of spherical codes and show they achieve a packing upper bound. We introduce a connection between tensor-spherical embeddings and adjacency matrices, showing that the former are generalizations of the latter with implications toward drastic compression.

In the second half, we analyze the memory and capacity of tensor-spherical embeddings and compare it to other bind-and-sum schemes, looking at their performance under two graph operations: vertex queries and edge composition. We focus on the Hadamard-Rademacher scheme as a competing method, which uses the Hadamard product and Rademacher vectors as the binding operation and vertex codes respectively. We demonstrate a tradeoff between memory and capacity in a binding operation’s compression, suggesting that compressed operations like the Hadamard product incur a proportional penalty in the number of edges they can store in superposition. Indeed, we show that the memory-capacity ratio of the tensor-spherical scheme matches that of the Hadamard-Rademacher scheme. Using the results established in the second half, we follow up on the connection to adjacency matrices in the first half, showing that tensor-spherical embeddings are drastic compressions of adjacency matrices and explore their utility in representing sparse matrices.

2 Previous Work

Bind-and-sum methods broadly fall under the field of hyperdimensional computing and vector symbolic architectures (VSAs) [8] [13][6] [24]. Vector symbolic architectures seek to imbue vector spaces with the ability to represent symbolic structures, and they usually consist of an encoding operator and binding operator. Objects are encoded as vectors through the former, and the symbolic binding of objects is represented by applying the binding operator to their vector codes. For example, after encoding the concepts *black* and *cat* as two vectors u and v , we can represent the tuple $(black, cat)$ via $u \otimes v$ where \otimes is the binding operator. Sets of objects are then represented by the superposition, or sum, of their vector codes. Going back to the previous example, we can represent the set $\{(black, cat), (brown, dog)\}$ as $u \otimes v + x \otimes y$, where *brown* and *dog* are encoded as x and y respectively.

The tensor product was first proposed by Smolensky [27] as a binding operation for representing general role-filler pairs. We study the tensor product in the context of graphs where the binding order is fixed and small, sidestepping a major issue where the tensor product’s dimension explodes with number of bound objects. Similarly, pseudo-orthogonal high-dimensional vectors have been proposed and explored by previous work [8] [13] [3] [28] and are a core component of hyperdimensional computing schemes. Spherical codes are one case of pseudo-orthogonal random vectors, and we study their synergistic pairing with the tensor product. Other works have also analyzed the capacities of different VSA schemes [4] and have given experimental comparisons between different schemes [26]. We restrict our analysis to the context of graphs and analyze graph operations that do not have analogues in a general VSA, such as edge composition.

As mentioned previously, the tensor-spherical embedding we study is a bind-and-sum graph embedding method, and many similar graph embedding methods have been proposed which use different binding and coding operations. Some use the circular correlation as a binding operation [21] [18], while others use the Hadamard product [25] [9] [23]. Many such methods use learned vertex codes [23] [21] [9], but in this paper we restrict ourselves to a random spherical codes. While some graph embedding works use tensor factorization to deconstruct the adjacency tensor [29] [20] [22], we have been unable to find another bind-and-sum graph embedding that use the tensor product as a binding operation. This might be due to its perceived memory cost relative to compressed bindings like the Hadamard product, but in this paper we shall challenge this perception.

Given the rich literature surrounding this problem, we believe our contribution is two-fold. Firstly, we provide a detailed analysis of the capabilities of tensor-spherical embeddings, as well as the tensor product and spherical codes individu-

ally. Interesting results include establishing a link between the tensor product and superposition, showing it is the most general therefore most expressive binding operation that respects superposition. Secondly, our analysis of the memory-capacity ratio and comparison to other bind-and-sum methods is novel, and indeed our results challenge common objections to the tensor product as too memory inefficient. We show that compressed binding operations suffer a proportionate penalty in their embedding’s capacity, suggesting that memory-efficient alternatives to the tensor product don’t actually offer any actual savings while sacrificing the expressivity of the tensor product. In conclusion, our contribution is our detailed analysis of the tensor-spherical embedding and, in particular, the many nice properties of the tensor product as a binding operation for graph embeddings.

3 Notation and Terminology

Our work focuses on embedding objects - vertices, edges, graphs - into vector spaces. Therefore, we shall denote the objects using bolded letters and their embeddings with the corresponding unbolded letter. For example, we denote a graph using \mathbf{G} and its embedding using G . In later sections, when there is no confusion we shall drop the distinction between the object and its embedding, using just the unbolded letter.

We also adopt graph terminology that may be non-standard for some readers. There are many names for the two vertices of a directed edge $(d, c) = d \rightarrow c$. In this paper, we shall call d the domain of the edge and c the codomain. Unless stated otherwise, all graphs will be directed graphs.

4 Embedding Method Overview

Given some set \mathbf{V} , we study a method for embedding the family of graphs that can be made from \mathbf{V} . Specifically, for any directed graph $\mathbf{G} = (\mathbf{V}_G, \mathbf{E}_G)$ such that $\mathbf{V}_G \subseteq \mathbf{V}$ and $\mathbf{E}_G \subseteq \mathbf{V} \times \mathbf{V}$, we embed \mathbf{G} by embedding its edge-set \mathbf{E}_G into a vector space. To this end, we first assign each vertex in \mathbf{V} to a d -dimensional unit vector, drawn independently and uniformly from the unit hypersphere \mathbb{S}^{d-1} . We then embed each directed edge (\mathbf{d}, \mathbf{c}) in the edgeset by the tensor product of their vertex embeddings:

$$(\mathbf{d}, \mathbf{c}) \mapsto d \otimes c$$

Fixing a basis, the tensor product is the outer product dc^T . Then, the embedding G of the graph \mathbf{G} - which we represent by its edgeset \mathbf{E}_G - is the sum of its edge

embeddings:

$$\mathbf{G} \mapsto G = \sum_i d_i \otimes c_i = \sum_i d_i c_i^T$$

Our embedding method can be separated into two parts: the spherical code used to embed vertices and the tensor product used to bind vertices into edges. We shall analyze each part separately as well as their synergistic pairing.

Finally, while we represent a graph \mathbf{G} by representing just its edgeset \mathbf{E}_G , we can also embed its vertex set by augmenting \mathbf{E}_G with self-loops (\mathbf{v}, \mathbf{v}) for each $\mathbf{v} \in \mathbf{V}_G$. This introduces confusion between a vertex and its self-loop, but for certain graphs, such as directed acyclic graphs, this is not a concern. However, we will focus on the original method of solely embedding the edgeset in this paper.

5 Graph Operations

In this section, we will give an overview of some core graph operations possible under the proposed embedding framework. One key property we require is that the vertex codes be (nearly) orthonormal vectors, and this is the primary motivation behind our use of spherical codes. Later sections will give a more precise analysis of near orthonormality, but for clarity we assume exactly orthonormal vertex codes in this section.

5.1 Edge Addition/Deletion

Adding/deleting the edge (a, b) to a graph corresponds to simply adding/subtracting ab^T from the graph embedding G .

5.2 Outbound/Inbound Vertices

For a given vertex d in G , suppose we wanted to find all the vertices c_i that a vertex d points to: (d, c_i) . To do this, we multiply G by d on the left:

$$d^T G = d^T \left(\sum_i d_i c_i^T \right) = \sum_i \langle d, d_i \rangle c_i^T = \sum_{d_i=d} c_i^T$$

In the last equality, we use the fact that the vertex embeddings are orthonormal. Since we represent sets as sums, this result is precisely the set of vertices that d points to.

Conversely, say we were interested in finding all vertices d_i that point to a vertex c : (d_i, c) . This would analogously correspond to right multiplying by c :

$$Gc = (\sum d_i c_i^T)c = \sum \langle c_i, c \rangle d_i = \sum_{c_i=c} d_i$$

We can generalize this to a set of candidate vertices. For example, we first represent a set of vertices S by the sum of its constituents $S = s_1 + \dots + s_n$. Then, to find all vertices in G that are connected to any vertex in S by an outbound edge, we multiply G on the right by S :

$$GS = (\sum d_i c_i^T)(s_1 + \dots + s_n) = \sum_{c_i \in S} d_i$$

Analogously, to find all vertices in G connected to S by an inbound edge, we multiply G on the left by S^T . All subsequent operations are also multilinear like the edge query, and so they can all be similarly extended to handle sets of vertices or edges. For simplicity, we will focus on just the singleton case from now on.

5.2.1 Edge/Node Queries

Combining the two operations above, checking if a graph G contains the edge (d, c) would correspond to multiplying G by d on the left and c on the right:

$$d^T G c = d^T (\sum d_i c_i^T) c = \sum \langle d, d_i \rangle \langle c, c_i \rangle = 1_{\{(d,c) \in E_G\}}$$

Now suppose G were augmented with self-loops for each vertex, where G contains the loop vv^T for each of its vertices v . One can use the above procedure to detect if G contains a given vertex.

5.3 Edge Composition, k-length Paths, and Graph Flow

We can also perform edge composition with the graph embeddings. For example, given edges (a, b) and (b', c) , we want to return the composite edge (a, c) only if $b = b'$. This can be done by matrix multiplication of the edge embeddings:

$$(ab^T)(b'c^T) = \langle b, b' \rangle ac^T = 1_{\{b=b'\}} ac^T$$

Therefore, we can compose all edges in a graph G by computing its second matrix power:

$$G^2 = (\sum d_i c_i^T)(\sum d_j c_j^T) = \sum_{i,j} \langle c_i, d_j \rangle d_i c_j^T = \sum_{c_i=d_j} d_i c_j^T$$

Generalizing to paths of length k , the matrix powers of G correspond to the sets of paths of a fixed length:

$$G^k = \{\text{all } k\text{-length paths in } G\}$$

We can combine this with vertex queries to compute graph flows. Say one wanted to know all vertices c that are reachable from starting vertex d by a path of length k . Then one would compute:

$$d^T G^k = d^T \left(\sum_{d_i=d} d_i c_i^T \right) (G)^{k-1} = \sum_{d_i=d} c_i^T (G^{k-1}) = \dots = \{c \text{ such that there is a } k\text{-length path } d \rightarrow c\}$$

An analogous operation exists for determining all vertices d that end up at final vertex c after a path of length k :

$$G^k c = \{d \text{ such that there is a } k\text{-length path } d \rightarrow c\}$$

5.4 Edge Flipping, Undirected Graphs, and Alternization

Given an edge (a, b) with representation ab^T , the representation of the flipped edge (b, a) is the transpose matrix:

$$ba^T = (ab^T)^T$$

Therefore, the embedding of the dual graph G^{op} - flipping all edges of G - is the transpose of G .

$$G^{op} = G^T$$

One interesting application of this property is to extend our current graph framework to undirected graphs using the un-normalized matrix symmetrization procedure:

$$G \mapsto G + G^T$$

This procedure may introduce double-counting of certain edges, but for certain graphs, like directed acyclic graphs, this is not an issue.

Symmetrization corresponds to making a graph undirected, and alternization also has a graph interpretation. Recall that the un-normalized alternization procedure is:

$$G \mapsto G - G^T$$

Alternization sends an edge ab^T to $a \wedge b = ab^T - ba^T$, and now when we take the transpose of the alternating edge $a \wedge b$ we have $(a \wedge b)^T = -(a \wedge b)$. Edges are now signed, where a negative sign reverses the direction of the edge. This leads to some interesting implications when interpreting coefficients of edges. For

example, subtracting an edge now corresponds to adding the opposite edge rather than just edge deletion, and this in turn gives a natural interpretation to the zero coefficient: an equal quantity of the forward and reverse edges. This in turn gives allows one to interpret a coefficient's magnitude as the net flow of some quantity, while the coefficient's sign represents the flow's direction.

5.5 Subsetting and Subgraphs

In a previous section, we saw that vertex queries can determine the vertices connected to or from a set of vertices $\mathbf{S} \subseteq \mathbf{V}$. Now, suppose we wanted to know the edges whose domain is in \mathbf{S} . Abusing notation, let S denote the matrix whose columns are the vertex embeddings $s \in S$, and let $P_S = SS^T$ be the associated projection matrix. To find all edges whose domain is in S , we compute:

$$P_S G = SS^T \left(\sum d_i c_i^T \right) = \sum \langle s_j, d_i \rangle s_j c_i^T = \sum 1_{\{s_j=d_i\}} s_j c_i^T = \sum_{d_i \in S} d_i c_i^T$$

Similarly, to find all edges whose codomain is in S , we compute:

$$G P_S = \left(\sum d_i c_i^T \right) SS^T = \sum \langle s_j, c_i \rangle d_i s_j^T = \sum 1_{\{s_j=c_i\}} d_i s_j^T = \sum_{c_i \in S} d_i c_i^T$$

Now, say we wanted to extract the full subgraph G_S of G , whose edges are those of G that have both domain and codomain in S . Combining the above two equations, this amounts to conjugating G with P_S :

$$G_S = P_S G P_S$$

5.5.1 Translation between Vertex Codes

Suppose we have two different vertex codes $\phi_1 : V \rightarrow V_1$ and $\phi_2 : V \rightarrow V_2$. For a graph G , we then have a graph embedding induced from each vertex code, denoted $\phi_1(G)$ and $\phi_2(G)$. There is a natural way to convert $\phi_1(G)$ to $\phi_2(G)$. Let Φ_1 be the matrix whose columns are the vertex codes $\{\phi(v_1), \phi(v_2), \dots\}$ in that order; let Φ_2 be the similarly defined matrix for ϕ_2 . Then, we have the transition map between vertex codes $\Psi : V_1 \rightarrow V_2$ represented by the matrix $\Phi_2 \Phi_1^T$:

$$\Psi : V_1 \rightarrow V_2 \quad ; \quad \phi_1(v_i) \mapsto \phi_2(v_i) \quad ; \quad \Psi = \Phi_2 \Phi_1^T$$

Then, the graph representations $\phi_1(G)$ and $\phi_2(G)$ follow the relation:

$$\phi_2(G) = \Psi \phi_1(G) \Psi^T$$

5.6 Counting via the Trace

The trace of a graph embedding G will count the number of self-loops in the graph:

$$\text{tr}(G) = \text{tr}(\sum d_i c_i^T) = \sum \langle d_i, c_i \rangle = \sum 1_{\{d_i=c_i\}}$$

This property can be used for many interesting graph operations.

5.6.1 Vertex Counting in Augmented Graphs

For a graph G whose edgeset set is augmented with the self-loops vv^T for every v in its vertex set V_G , the trace will naturally return the cardinality of its vertex set:

$$\text{tr}(G) = \text{tr}(\sum d_i c_i^T) = \sum \langle d_i, c_i \rangle = |V_G|$$

5.6.2 Edge Counting and a Natural Metric

To count the number of edges in a graph $G = \sum d_i c_i^T$, one computes:

$$\text{tr}(G^T G) = \text{tr}((\sum c_i d_i^T)(\sum d_j c_j^T)) = \text{tr}(\sum \langle d_i, d_j \rangle c_i c_j^T) = \sum \langle d_i, d_j \rangle \langle c_i, c_j \rangle = |E_G|$$

This gives a nice relation to the Frobenius norm $\|\cdot\|_F$ via the identity $\|A\|_F^2 = \text{tr}(A^T A)$. This shows that the squared Frobenius norm of a graph representation is precisely the cardinality of its edge set. Hence, the natural metric on our graph embeddings would be the one induced from the Frobenius norm:

$$d(G, H) := \|G - H\|_F = \sqrt{\# \text{ of different edges}}$$

where this metric depends solely on the number of different edges between the two graphs.

5.6.3 Testing Graph Homomorphisms

Finally, one interesting application of the trace is to quantify the 'goodness' of a proposed graph homomorphism. Recall that a graph homomorphism f from graph G to graph H is comprised of a vertex function $f_1 : V_G \rightarrow V_H$ and edge function $f_2 : E_G \rightarrow E_H$ such that every edge (a, b) is mapped by f_2 to the edge $(f_1(a), f_1(b))$. Hence, every homomorphism is completely determined by its vertex function, and so it suffices to test if a vertex function $f : V_G \rightarrow V_H$ induces a graph homomorphism. Therefore, for every proposed vertex function f we assign a quantity called the graph homomorphism coefficient, described in detail below.

Given two graphs $G = \sum d_i c_i^T$ and $H = \sum a_j b_j^T$ with proposed vertex function $f : V_G \rightarrow V_H$, the vertex function f induces the following map:

$$G = \sum d_i c_i^T \mapsto \sum f(d_i) f(c_i)^T = f(G)$$

Note that $f(G)$ can be computed using the method mentioned in the previous section. If f is truly a graph homomorphism, then $f(G)$ is a subgraph of H and every edge of $f(G)$ is an edge of H . We therefore compute the number of matching edges between $f(G)$ and H , denoted δ_f :

$$\delta_f = \text{tr}(f(G)^T H) = \text{tr}((\sum f(c_i) f(d_i)^T)(\sum a_j b_j^T)) = \sum \langle f(d_i), a_j \rangle \langle f(c_i), b_j \rangle$$

Dividing δ_f by $|E_G| = \text{tr}(G^T G)$ gives the fraction of edges in $f(G)$ that have matches in H . We call this ratio the graph homomorphism coefficient, denoted as $\Delta_f := \frac{\delta_f}{|E_G|}$. Note that $\Delta_f \in [0, 1]$. If f truly induces a graph homomorphism, then every edge has a match and $\Delta_f = 1$; conversely, if $f(G)$ has no matching edges in H , then $f(G)$ is totally different from H and $\Delta_f = 0$. In this sense, the graph homomorphism coefficient gives a measure of how close a vertex function f is to inducing a graph homomorphism.

5.7 Vertex Degree and Gram Matrices

In a directed graph G , consider a fixed vertex v . The in-degree of v , $\text{in}(v)$, is the number of edges that go into v - ie. have codomain v . Similarly, the out-degree of v , $\text{out}(v)$, is the number of edges that go out of v - ie. have domain v . Generalizing these definitions, we define the joint in-degree of two vertices v and w , $\text{in}(v, w)$, as the number of vertices d_i that have both an edge into v and an edge into w . The joint out-degree of two vertices v and w , $\text{out}(v, w)$, is similarly defined. Note that using the generalized definitions, the in/out-degree of a vertex with itself coincides with the single-case definition. Using our graph embeddings, there is a natural way to compute both of these degrees.

We first handle the in-degree of a vertex. Recall that Gv is the superposition, or sum, of all vertices d_i that go into v with an edge (d_i, v) . Since vertex codes are orthonormal, we can use the squared Euclidean norm to count the number of vertices in superposition:

$$\|Gv\|^2 = (Gv)^T Gv = v^T (G^T G)v = \text{in}(v)$$

In fact, for two vertices v and w , we again appeal to orthonormality of the vertex codes to compute their joint in-degree:

$$(Gv)^T Gw = v^T (G^T G)w = \text{in}(v, w)$$

Thus, we see that the Gram matrix $G^T G$ represents a bilinear form that computes the joint in-degree of two vertices:

$$G^T G : V \times V \rightarrow \mathbb{R} \quad ; \quad v \times w \mapsto v^T (G^T G) w = in(v, w)$$

We shall call the gram matrix $G^T G$ the in-degree matrix.

A similar line of reasoning shows that the Gram matrix $G G^T$ computes the joint out-degree between two vertices. Hence, we shall call $G G^T$ the out-degree matrix. Immediately, one natural question when working with Gram matrices are their spectral properties. Indeed, there are natural links to properties of graph connectivity, which we discuss in the next section.

5.8 Graph Connectivity

We embed a graph G as a matrix $\mathbb{R}^{d \times d} \cong V \otimes V$, and so we may view each graph embedding as a linear operator on the vertex code space V . This perspective yields some interesting links to the connectivity properties of graphs.

5.8.1 Invariant Subspaces and Connected Components of Undirected Graphs

Given a linear operator $T : V \rightarrow V$, a subspace $W \subseteq V$ is an invariant subspace of T if $T(W) \subseteq W$. An invariant subspace W is irreducible if it contains no non-trivial invariant subspace. Now, consider a directed acyclic graph G , its dual G^T , and a subset of its vertices $\{v_1, \dots, v_n\} \subseteq V_G$. Let $W = span(\{v_1, \dots, v_n\})$, and let $U(G) = G + G^T$ be its induced undirected graph.

Suppose W were an invariant subspace of G , or equivalently $Gv_i \in W$ for all v_i . As Gv_i is the sum of all vertices d_j that connect to v_i via an outbound edge, this means that the only in-bound connections to $\{v_1, \dots, v_n\}$ are from its members. Similarly, the condition that W be an invariant subspace of G^T is equivalent with the condition the only out-bound edges to $\{v_1, \dots, v_n\}$ are from its members. Then, if we consider the induced undirected graph $U(G)$, W is an invariant subspace iff all paths starting at any v_i terminate at some other v_j . Hence, W is an invariant subspace iff the underlying set of vertices $\{v_1, \dots, v_n\}$ is a union of connected components of $U(G)$. Immediately, $\{v_1, \dots, v_n\}$ is a connected component iff W is an irreducible invariant subspace. These are the weakly connected components of the directed acyclic graph G .

6 Derivation of the Tensor Product

In this section, we derive the tensor product binding from superposition principle and show it is the most general embedding method. We also give an alternative derivation of the tensor product and orthonormality when considering suitability toward certain graph operations.

6.1 Superposition and the Tensor Product

We shall derive the tensor product from the superposition principle, which states that a set's vector code is the sum of its members' vector codes. Indeed, along the way we shall establish the following connection between the superposition principle and the tensor product:

Theorem 6.1. *For any fixed vertex code $\phi : \mathbf{V} \rightarrow V$, let $\psi : V \times V \rightarrow \mathbb{R}^n$ be any binding operation that respects superposition. Then the resulting bound code $\psi(V, V)$ has a unique linear derivation from the tensor product $V \otimes V$. In this sense, the tensor product is the most general binding operation.*

Proof. Assume we are given a vertex code $\phi : \mathbf{V} \rightarrow V$. Given a directed graph $G = (V_G, E_G)$ in V , our task is to represent G by embedding edge set E_G via a superposition of its edges. First, suppose G has multiple edges from a common domain $\{d\}$ to multiple codomains $\{c_1, \dots, c_k\}$:

$$\{(d, c_1), \dots, (d, c_k)\} = \bigcup_i \{(d, c_i)\}$$

Similarly, consider the reverse situation to multiple domains with a single codomain. Then, any edge embedding $\psi : V \times V \rightarrow \mathbb{R}^n$ that respects superposition must satisfy the following two equations:

$$\begin{aligned} \psi(\{(d, c_1), \dots, (d, c_k)\}) &= \sum \psi(\{(d, c_i)\}) \\ \psi(\{(d_1, c), \dots, (d_l, c)\}) &= \sum \psi(\{(d_j, c)\}) \end{aligned}$$

Thus, ψ induces a bilinear function $\tilde{\psi}$ on the vertex code via:

$$\begin{aligned} \tilde{\psi} : V \times V &\rightarrow \mathbb{R}^n \\ (\phi(v), \phi(w)) &\mapsto \psi(v, w) \end{aligned}$$

By the universality of the tensor product [14], the bilinear $\tilde{\psi}$ map has a corresponding unique linear map $\psi^* : V \otimes V \rightarrow \mathbb{R}^n$, and so the tensor product uniquely maps into every edge embedding that respects superposition. \square

For example, three common alternative binding operations - Hadamard product, convolution, and circular correlation - all are linearly induced from the tensor product. Representing the tensor product as the outer product matrix, the Hadamard product is the diagonal of the matrix while the convolution and circular correlation are sums along pairs of diagonals. Therefore, given a vertex code ϕ we may as well consider its natural induced edge embedding under the tensor product.

6.2 Derivation from Graph Operations

In this section, we show that the tensor product and orthonormal codes can be naturally derived when considering suitability toward graph operations. While we can analyze many possible graph operations and still get the same result, for brevity we shall focus on the edge query function Q :

$$Q : (V \times G) \rightarrow V$$

The edge query inputs a vertex-graph pair (v, G) and returns all the vertices that v points to. We shall consider a general edge-binding operation ψ and denote edges under this binding operation as $\psi(v, w)$. As usual, we assume that both Q and ψ respect superposition.

Since Q respects superposition and hence is a multilinear function, we can completely characterize it by considering its actions on some basis set $b_i \times \psi(b_j, b_k)$. Let us assume some subset of vertex embeddings form a basis for V , and let us examine Q applied to a single edge: $Q(u, \psi(v, w))$. For notational simplicity, we will drop the ψ and just represent edges as tuples (v, w) . Ideally, we want:

$$Q(u, (v, w)) = \begin{cases} w & u = v \\ 0 & u \neq v \end{cases}$$

However, this condition makes Q a non-linear function. Instead, the 'closer' u is to v , we want the output of Q to be closer to w ; on the other hand, if u is totally 'different' from v , we want the query function to return nothing: the zero vector. In fact, let us fix w , so now the function has just two arguments:

$$Q(-, (-, w)) = Q_w(-, -)$$

By fixing w , in light of the previous discussion we see that Q_w interpolates between w and 0 depending on the similarity of its two arguments. Equivalently, this means we can factorize Q_w into a similarity function S multiplying w , where the output of S is in $[0, 1]$.

$$Q_w(-, -) = S(-, -)w$$

The similarity function S checks for agreement between query vertex u and source vertex v , and the closer they are the closer the output is to w . Ideally, we want S to return 1 (and hence an output of w) whenever $u = v$:

$$S(u, v) = 1 \quad \text{if } u = v$$

There is one more thing we need to consider: orthogonal decomposition. Consider the orthogonal projection of v onto u : $v = v_u + v_u^\perp$. By linearity, our similarity function becomes:

$$S(u, v) = S(u, v_u) + S(u, v_u^\perp) = \frac{\langle u, v \rangle}{\langle u, u \rangle} S(u, u) + S(u, v_u^\perp)$$

Consider the second term $S(u, v_u^\perp)$. It is natural that this term be 0, since these two vectors are entirely different. Earlier we stated that $S(u, u) = 1$, so our similarity function becomes:

$$S(u, v) = \frac{\langle u, v \rangle}{\langle u, u \rangle}$$

We can arbitrarily scale S by some constant and shrink u by that same constant without affecting the outcome, so for convenience let us now assume all vertices are unit vectors. Then, our similarity function becomes:

$$S(u, v) = \langle u, v \rangle$$

Picking any unit basis $\{b_i\}$ of V and applying the same analysis to all pairs of basis vectors, we come to the general equation:

$$S(b_i, b_j) = \langle b_i, b_j \rangle$$

By linearity this completely determines S , and so S is just the usual dot product.

Having determined the form of S , our query function Q can now be expressed as:

$$Q(u, (v, w)) = \langle u, v \rangle w$$

This holds for any w , and so by multilinearity our query function takes the form:

$$Q(\sum_i u_i, \sum_j (v_j, w_j)) = \sum_i (\sum_j \langle u_i, v_j \rangle w_j) = \sum_i u_i^T (\sum_j v_j w_j^T)$$

Focusing on the graph term $\sum_j v_j w_j^T$, we see this is the graph embedding using the tensor product as a binding operation. To summarize, we derived the form the

edge query Q should take using multilinearity and some natural desiderata, and this natural form is a linear computation involving the tensor product. Hence, regardless of the binding method ψ , the query function Q can be equivalently computed using tensor product graph embeddings. Moreover, assuming normalized codes the natural similarity function is the dot product, and this suggests orthonormality is needed to distinguish between vertex codes.

Considering just the edge query function, we naturally derive our graph embedding scheme. In fact, this derivation is connected to superposition and multilinearity. Any graph operation that respects superposition must be linear in each argument; as all multilinear functions filter uniquely through the tensor product, all natural graph operations can be derived from corresponding operations on the tensor product. Thus, we could similarly derive the tensor product when considering any other graph operation, as long as it respects superposition.

7 Spherical Codes and Approximate Orthonormality

In previous sections, we assumed our vertex codes to be exactly orthonormal. However, this orthonormality requirement is not efficient in the number of codes we can pack into a space, since we can pack at most d orthonormal vectors into a d -dimensional space. Instead, we relax the requirement of strict orthonormality and use approximately orthonormal spherical codes. Two natural questions arise: how many pseudo-orthonormal vectors can one pack into \mathbb{R}^d , and how close do spherical codes come to achieving this limit? In this section we shall answer these two questions and give an account of approximate orthonormality in high dimensions.

7.1 Packing Upper Bounds

First, we give an upper bound on the number of approximately orthonormal vectors one can pack in \mathbb{R}^d . To make approximate orthonormality precise, we say the unit vectors u, v are ϵ -orthogonal if $|\langle u, v \rangle| < \epsilon$. The Johnson-Lindenstrauss Theorem [7] implies a packing upper bound, which is shown to be tight [15].

Theorem 7.1 (Johnson-Lindenstrauss). *Let $x_1, \dots, x_m \in \mathbb{R}^N$ and $\epsilon \in (0, 1)$. If $d > \frac{8 \ln(m)}{\epsilon^2}$, then there exists a linear map $f : \mathbb{R}^N \rightarrow \mathbb{R}^d$ such that for every x_i, x_j :*

$$(1 - \epsilon) \|x_i - x_j\|^2 \leq \|f(x_i) - f(x_j)\|^2 \leq (1 + \epsilon) \|x_i - x_j\|^2$$

Corollary 7.1.1. *For any $\epsilon \in (0, \frac{1}{2})$, one can pack at most $O(e^{C d \epsilon^2})$ ϵ -orthogonal unit vectors in \mathbb{R}^d for some universal constant C .*

Proof. Let m be any integer such that $d > \frac{8\ln(m+1)}{\epsilon^2}$. Consider the set of $(m+1)$ vectors $\{e_1, \dots, e_m, 0\}$ in \mathbb{R}^m . These satisfy the conditions of the Johnson-Lindenstrauss Theorem, and let f be the JL map. Then,

$$(1 - \epsilon) = (1 - \epsilon)\|x_i\|^2 \leq \|f(x_i) - 0\|^2 = \|f(x_i)\|^2 \leq (1 + \epsilon)$$

Hence, since $\|e_i - e_j\|^2 = 2$ for $i \neq j$:

$$2(1 - \epsilon) \leq \|f(e_i) - f(e_j)\|^2 = \|f(e_i)\|^2 + \|f(e_j)\|^2 - 2\langle f(e_i), f(e_j) \rangle \leq 2(1 + \epsilon)$$

Plugging the first equation to the second, we have:

$$-2\epsilon \leq \langle f(e_i), f(e_j) \rangle \leq 2\epsilon$$

Thus, using $u_i = \frac{f(e_i)}{\|f(e_i)\|}$, the first equation, and the fact that $\epsilon < \frac{1}{2}$:

$$-4\epsilon \leq -\frac{2\epsilon}{(1 - \epsilon)} \leq \langle u_i, u_j \rangle \leq \frac{2\epsilon}{1 - \epsilon} \leq 4\epsilon$$

Therefore we have:

$$D > 8\ln(m+1)/\epsilon^2 \implies m = O(e^{Cd\epsilon^2})$$

for some constant C . □

7.2 Spherical Codes

We use spherical codes, which are random vectors drawn uniformly from the d -dimensional unit hypersphere \mathbb{S}^{d-1} , to generate approximately orthonormal vertex codes. In this section, we give the exact distribution of their dot product and show that they achieve the packing upper bound in Corollary 7.1.1.

7.2.1 Distribution of the Dot Product

Theorem 7.2. *If u, v are uniformly distributed over \mathbb{S}^{d-1} , let $X = \langle u, v \rangle$ and $Y = \frac{X+1}{2}$. Then, Y follows a $\text{Beta}(\frac{d-1}{2}, \frac{d-1}{2})$ distribution.*

Proof. Since both u and v are uniformly distributed over \mathbb{S}^{d-1} , by symmetry we may fix v as any unit vector without changing the distribution of X . Hence, let v be the first coordinate vector e_1 , and so $X = \langle u, e_1 \rangle$. The set of vectors u such that $\langle u, e_1 \rangle = x$ form a spherical section of \mathbb{S}^{d-1} : a $(d-1)$ -sphere of radius $\sqrt{1-x^2}$. Then, the set of vectors with dot product $x \leq X \leq x + \delta$ corresponds to a d -dimensional belt on the sphere. Since the probability of a set is proportional to its surface area, $P(x \leq X \leq x + \delta)$ is proportional to the surface area of this

belt. The area of a d -dimensional sphere of radius r is Cr^{d-1} for some constant C , and if $\theta = \cos^{-1}(X)$ we have:

$$\begin{aligned} P(x \leq X \leq x + \delta) &\propto \int_{\cos^{-1}(x)}^{\cos^{-1}(x+\delta)} (\sqrt{1 - \cos^2(\theta)})^{d-2} d\theta \\ &= \int_x^{x+\delta} (\sqrt{1 - t^2})^{d-2} d(\cos^{-1} t) \propto \int_x^{x+\delta} (1 - t^2)^{\frac{d-3}{2}} dt \end{aligned}$$

Hence, if f_X is the density of X , $f_X \propto (1 - x^2)^{\frac{d-3}{2}}$. Then, letting $X + 1 = 2Y$, we can simplify:

$$(1 - x^2)^{\frac{d-3}{2}} = (1 - x)^{\frac{d-3}{2}} (1 + x)^{\frac{d-3}{2}} = (2 - 2y)^{\frac{d-3}{2}} (2y)^{\frac{d-3}{2}} \propto (1 - y)^{\frac{d-3}{2}} y^{\frac{d-3}{2}}$$

Thus, $Y = \frac{X+1}{2}$ follows a Beta($\frac{d-1}{2}, \frac{d-1}{2}$) distribution \square

Corollary 7.2.1. *The dot product X between u, v , uniformly distributed over \mathbb{S}^{d-1} , has $E(X) = 0$ and $Var(X) = \frac{1}{d}$.*

7.2.2 Optimality of Spherical Codes

Now, given a set of k spherical codes, we want to ensure that all of them are approximately orthonormal. Surprisingly, we shall see that for a fixed probability of violating ϵ -orthonormality, the number of spherical codes k will be $O(e^{Cde^2})$ for some universal constant C , matching our upper bound.

Theorem 7.3. *For k vectors x_1, \dots, x_k sampled iid from the uniform distribution on \mathbb{S}^{d-1} and for any $\epsilon > 0$, we have:*

$$\max_{i \neq j} |\langle x_i, x_j \rangle| < \epsilon$$

with probability at least $1 - 2\binom{k}{2}e^{-\frac{d}{2}\epsilon^2}$

Proof. From Corollary 7.2.1, the dot product X is a random variable bounded absolutely by 1 and with variance $\frac{1}{d}$. Hence, Bernstein's inequality [2] gives:

$$\begin{aligned} P(|X| > \epsilon) &= 2P(X > \epsilon) \quad X \text{ is symmetrically distributed about } 0 \\ &\leq 2e^{\epsilon^2/(\frac{2}{d} + \frac{2\epsilon}{3})} \quad \text{Bernstein's inequality} \\ &\leq 2e^{\epsilon^2/\frac{2}{d}} \\ &= 2e^{\frac{d}{2}\epsilon^2} \end{aligned}$$

Using a union bound over all $\binom{k}{2}$ pairs gives the result. \square

Hence, for a fixed error threshold T , we can choose the maximum number of vectors k such that the error probability is less than T :

$$T \approx C_1 \binom{k}{2} e^{-C_2 d \epsilon^2} \implies k \approx O(e^{C_3 d \epsilon^2})$$

for universal constants C_1, C_2, C_3 . This matches the upper bound given by Theorem 7.1, and spherical codes achieve the packing upper bound in Corollary 7.1.1.

8 Alternative Binding Operations

Our graph embedding method uses the tensor product to bind vertex codes into an edge. However, this means that the graph embedding space scales quadratically with the vertex code dimension, and in response various memory efficient alternatives have been proposed. In this section, we shall primarily analyze three prominent alternative binding operations: the Hadamard product, convolution, and circular correlation. This, in addition to Section 9, will prepare us to analyze other bind-and-sum embeddings and compare them to tensor-spherical embeddings.

8.1 Hadamard Product

The Hadamard product of two vectors a and b , denoted $a \odot b$, is their element-wise multiplication:

$$[a \odot b]_k = a_k b_k$$

It preserves the dimension of the vertex code and scales linearly with the code dimension. The most common vertex codes when using the Hadamard product are phasor codes and binary codes: vectors whose entries are the complex and real units respectively. These codes have nice unbinding operations with respect to the Hadamard product, where multiplication by the conjugate of a vertex code will remove that code from the binding:

$$\bar{a} \odot (a \odot b) = b$$

In the next section, we also briefly touch on other codes. However, we shall see that since unbinding the Hadamard product requires element-wise division, many choices of random codes are not suitable for accurate graph operations.

8.2 Convolution

The convolution of two vectors a and b , denoted $a * b$, is defined as:

$$[a * b]_k = \sum_i a_i b_{k-i}$$

If \mathcal{F} denotes the Fourier transform, then the convolution can also be expressed as:

$$a * b = \mathcal{F}^{-1}(\mathcal{F}(a) \odot \mathcal{F}(b))$$

Hence, convolution and the Hadamard product are equivalent up to a Hermitian change of basis, and so it is sufficient to analyze just the Hadamard product. Indeed, common codes used with convolution are those whose Fourier transforms are phasor and binary codes, and there is a bijection between the codes used for convolution and codes used for the Hadamard product.

8.3 Circular Correlation

The circular correlation of two vectors a and b , denoted $a \star b$, is defined as:

$$[a \star b]_k = \sum_i a_i b_{k+i}$$

Using the Fourier transform, the circular correlation also can be expressed as:

$$a \star b = \mathcal{F}^{-1}(\overline{\mathcal{F}(a)} \odot \mathcal{F}(b))$$

For a vector a , let y_k be the k^{th} Fourier coefficient of a :

$$y_k = \sum_{s=0}^{n-1} \exp\left(\frac{2\pi i(-ks)}{n}\right) a_s$$

Taking the conjugate, we get:

$$\overline{y_k} = \sum_{s=0}^{n-1} \exp\left(\frac{2\pi i(ks)}{n}\right) a_s = \sum_{s'=0}^{n-1} \exp\left(\frac{2\pi i(-ks')}{n}\right) a_{-s'}$$

Hence, $\mathcal{F}^{-1}(\overline{\mathcal{F}a}) = Pa$, where P is the permutation that flips indices, and so the circular correlation is convolution augmented with flipping the first argument. This is a special case of using permutation to induce ordered bindings, which we shall cover in the next subsection. Since the circular correlation is a permuted convolution and convolution is equivalent to the Hadamard product, it is sufficient to study the Hadamard product with permutations.

8.4 Alternative Bindings as Compressions of the Tensor Product

As noted in our derivation of the tensor product from superposition, the tensor product is a universal construction. That is, every binding method that respects superposition - bilinearity - is linearly induced from the tensor product. The three alternative binding operations - the Hadamard product, convolution, circular correlation- are no exception.

More specifically, fixing the standard basis the tensor product $v \otimes w$ is the outer product vw^T , a $d \times d$ matrix. The Hadamard product is the main diagonal of this matrix. Similarly, the entries of the circular correlation are sums along pairs of diagonals of vw^T , spaced by an interval of $2(d - 1)$. For convolution, we analogously take sums along pairs of the reverse diagonals (bottom left to top right).

Hence, all three operations can be seen as compressions of the tensor product, where we compress a $d \times d$ matrix into a d -dimensional vector. While on the surface this might seem to save much in terms of memory, in the next subsection we shall see these compressed binding operations are unable to perform some fundamental graph operations. Moreover, in Sections 10 and 11 we show that the Hadamard product's compression incurs a proportionate penalty in the number of edges it can accurately store in superposition, meaning it offers no real savings in memory.

8.5 Hadamard Product: Graph Functionality

As established in the preceding subsections, all three operations are, up to a Hermitian change of basis, equivalent to the Hadamard product with possibly a permutation applied to one of its arguments. Hence, in this section we shall analyze the Hadamard product and its suitability for graph embeddings.

Firstly, the Hadamard product can perform edge composition when used in conjunction with binary codes. This is because it has easy unbinding operations, where multiplication by a code will remove that code from the binding. Using Hadamard-binary embeddings, we can perform edge composition by taking the Hadamard product of two edges:

$$(a \odot b) \odot (b \odot c) = a \odot c$$

Moreover, note that in the case of a mismatch between the vertices, the resulting edge is:

$$(a \odot b) \odot (b' \odot c) = a \odot c \odot n$$

where n is a noisy binary code. Importantly, there is no destruction of mismatched edges during edge composition. This will impact the number of edges we can accurately store in superposition, which we shall cover in Section 11.

One can ask if there is any alternative edge composition function that is better suited for the Hadamard product. Assuming this edge composition function respects superposition, one can show that the natural edge composition function under the Hadamard product is again the Hadamard product. We give a sketch of the argument: firstly, the desired composition function respects superposition, so it is a multilinear function and is completely determined by its action on some basis $\{b_i\}$. Fixing the standard basis, we impose the natural constraint:

$$(e_i \odot e_j) \times (e_k \odot e_l) \mapsto \begin{cases} e_i \odot e_l & j = k \\ 0 & j \neq k \end{cases}$$

Since these constraints are satisfied by the Hadamard product, the edge composition function must be the Hadamard product.

The Hadamard product is unable to represent directed edges because it is symmetric: $a \odot b = b \odot a$. A common fix is to permute one of its arguments before binding, so now we bind as $Pa \odot b$ where P is some permutation matrix. Our augmented binding operation becomes:

$$(a, b) \mapsto Pa \odot b$$

This augmented operation is certainly able to represent directed edges, but it is now unable to perform edge composition. Disregarding oracle operations where one already knows the bound vertices, using the Hadamard product to perform edge composition results in:

$$(Pa \odot b) \odot (Pb \odot c) = a \odot c \odot (b \odot Pb)$$

The noise term $(b \odot Pb)$ will not cancel unless P is the identity, the non-permuted case. A similar question arises whether there is a better edge composition function for the permuted Hadamard: assuming this edge composition function respects superposition, by multilinearity one can show no such operation exists. Intuitively, one would like to send the pair (Pa, a) to the vector of all ones, but the symmetry in the Hadamard product and its compression means such a map is not possible without breaking multilinearity.

In summary, we see that the Hadamard product with binary codes sacrifices some core graph functionality: with the regular Hadamard product, one can perform edge composition but cannot represent directed edges; in the permuted case, one can represent directed edges but cannot perform edge composition. One can show

that other core graph operations, like subsetting and graph homomorphisms, are also impossible under such schemes. Thus, in the Hadamard-binary case we see that it cannot represent graph operations that the tensor product can.

8.5.1 Hadamard Product: Phasor Codes

Phasor codes, which generalize binary codes, are even less suitable than binary codes. The natural unbinding operation for phasor codes is to multiply by the conjugate codes. However, this already makes it unsuitable for edge composition in both the non-permuted and permuted case. In the non-permuted case:

$$\overline{(a \odot b)} \odot (b \odot c) = \bar{a} \odot c \neq a \odot c$$

The permuted case has a similar deficiency. Again due to the compression of the Hadamard product, there is no multilinear function that conjugates just one argument of the bound edge $a \odot b$. Intuitively, this is due to the symmetry of the Hadamard product, since it is unable to distinguish which particular vertex to conjugate. Edge composition using phasor codes is impossible, and any code which can be derived from the phasor code suffers a similar defect.

8.6 Hadamard Product: Continuous Codes

Similarly, since unbinding the Hadamard product requires element-wise division, many choices of random continuous codes are numerically unstable. In fact, the next section we shall see that specific cases of continuous codes all suffer from having infinite moments, making accurate graph operations impossible since the noise terms will overwhelm the signal. Moreover, operations like edge composition are also impossible for similar reasons as the phasor code, where one needs invert a specific vertex of the bound edge. Due to the Hadamard product's compression, such a multilinear map does not exist.

9 Random Codes

In this section, we state and establish some basic results of various random codes in preparation of our analysis of other bind-and-sum approaches. Throughout this section we assume all vertex codes have common dimension d .

9.1 Spherical Codes

We generate spherical codes by sampling iid from the d -dimensional unit hypersphere \mathcal{S}^{d-1} . They have the following properties:

Theorem 9.1 (Spherical Code Properties). *Let X denote the dot product between two spherical codes. Then, the following statements hold:*

1. $\frac{X+1}{2} \sim \text{Beta}(\frac{d-1}{2}, \frac{d-1}{2})$
2. $E(X) = 0$ and $\text{Var}(X) = \frac{1}{d}$
3. $|X| \propto \frac{1}{\sqrt{d}}$ with high probability.

Proof. The first two claims follow from the results of Theorem 7.2 and Corollary 7.2.1. The final claim follows from either Bernstein's inequality or a Gaussian approximation. \square

9.2 Rademacher Codes

Rademacher codes are vectors v where each entry is an iid Rademacher random variable: $v_i = \pm 1$ with probability $\frac{1}{2}$. They have the following properties.

Theorem 9.2 (Rademacher Code Properties). *Let X denote the dot product of two Rademacher vectors. The following statements hold:*

1. $\frac{X+d}{2} \sim \text{Binomial}(d, \frac{1}{2})$
2. $EX = 0$ and $\text{Var}(X) = d$
3. $X \propto \sqrt{d}$ with high probability.

Proof. Since the product of two Rademacher random variables, X is the sum of d Rademacher random variables. If $B = \text{Bernoulli}(\frac{1}{2})$, then $2B - 1$ is a Rademacher random variable. Hence, the sum of d Rademacher is $2Y - d$ where $Y \sim \text{Binomial}(d, \frac{1}{2})$ and so $X = 2Y - d$. This establishes the first statement, and the second statement follows from the first. The third claim follows from a Chernoff inequality [2] or a Gaussian approximation. \square

9.3 Other Continuous Codes

Here, we will briefly describe three common continuous codes: Gaussian, Cauchy, and uniform vectors. The entries of Gaussian vectors are iid Gaussian, usually the standard Gaussian. Cauchy and uniform vectors are analogously generated, with their entries being drawn from the standard Cauchy and $\text{Unif}[0, 1]$ respectively. The main problem with these codes is that unbinding the Hadamard product requires element-wise division, and the resulting ratios of random variables will have infinite moments. This results in ill-controlled noise terms and makes them unsuitable for accurate graph operations.

Theorem 9.3. *For t, u iid Gaussian, Cauchy, or uniform. Let $Y = \frac{t}{u}$. Then, for any of the three distributions, all moments of Y are undefined.*

Proof. In the Gaussian case, the ratio of two independent standard Gaussians is a Cauchy random variable, which is known to have infinite moments. In the Cauchy case, the ratio of two independent standard Cauchy rv's has the density [10]:

$$f_{Y_c}(y) \propto \frac{1}{(y^2 - 1)} \ln(y^2)$$

Then, comparing integrals:

$$\infty = \frac{1}{2} \int_0^c |\ln(y^2)| \leq \int_0^c y f_{Y_c}(y) \leq \int_0^\infty y f_{Y_c}(y)$$

we see that the first moment is also undefined (for some sufficiently small constant c). In the uniform case, the ratio of two independent $U[0, 1]$ rv's has the following density [19]:

$$f_{Y_u}(y) = \begin{cases} \frac{1}{2} & 0 < y < 1 \\ \frac{1}{2y^2} & y \geq 1 \\ 0 & y \leq 0 \end{cases}$$

A similar comparison test also shows that the first moment is undefined. Thus, the first moment, and hence all moments, are undefined for all three choices of distribution. \square

10 Binding Comparison: Edge Queries

In Section 8, we showed the the convolution and circular correlation are special cases of the Hadamard product. Similarly in Section 9, we found that binary codes have most representational power of the suitable codes considered. Hence, we shall primarily compare the memory and capacity of the tensor-spherical scheme to the Hadamard-Rademacher scheme. We also briefly consider other continuous coding schemes paired with the Hadamard product, but we shall see that they are too noisy for accurate graph operations.

In this section, we focus on the edge query: given a graph embedding, we determine whether it contains a specific edge. For each bind-and-sum scheme considered, we analyze how the dimension of the embedding (memory) and number of edges in superposition (capacity) affect the accuracy of correctly retrieving the right edge from a graph embedding.

10.1 Overview

We denote the edge binding operation as ψ , which can be either the Hadamard product or the tensor product. Let us work with the following fixed graph:

$$G = \psi(v, u) + \sum_{i=1}^k \psi(q_i, r_i)$$

where all the q, r 's are distinct from u, v . We will perform an edge query that seeks to find the vertices in G that vertex v points to (or is connected to in the undirected case).

10.2 Hadamard Product and Rademacher Codes

We first look at the Rademacher-Hadamard scheme, analyzing both the magnitude of the error term as well as bounding the probability of retrieving the correct vertex.

10.2.1 Error Norms

In this case, our edge query is of the form:

$$Q(v, G) = v \odot (v \odot u + \sum_{i=1}^k q_i \odot r_i) = u + \sum_{i=1}^k q_i \odot r_i \odot v$$

Since the product of Rademacher's is still Rademacher, we see that each term $q_i \odot r_i \odot u = s_i$ is still a Rademacher random vector. We can express the output as:

$$Q(v, G) = u + \sum_{i=1}^k s_i$$

Thus, the result of our query can be split into the correct signal u and a noise term ϵ , which is a sum of k independent Rademachers. We then have the following result on their expected magnitudes.

Theorem 10.1 (Hadamard-Rademacher Signal-to-Noise). *When performing a edge query with a single correct vertex u , under the Hadamard product and Rademacher codes of dimension d we have:*

1. *The squared norm of the signal $E||u||^2$ is d .*
2. *The squared norm of the noise $E||\sum_{i=1}^k s_i||^2$ is kd*
3. *The signal-to-noise ratio is $\frac{1}{k}$*

Proof. Let us consider the norm of the noise term $\sum_{i=1}^k r_i$ relative to the signal u . Then, using the results from Section 9.2 and independence, we see that:

$$E||u||^2 = d \quad ; \quad E||\sum_{i=1}^k r_i||^2 = \sum_i E||r_i||^2 + \sum_{j \neq k} E\langle r_j, r_k \rangle = kd$$

Hence, their ratio is $\frac{1}{k}$ □

Note that we assumed that all the edges were generated by independently sampling Rademacher codes, and hence precludes the possibility of a vertex participating in more than one edge. However, note that we can write the graph embedding into a sum of subgraphs such that each subgraph has edges whose vertices are all distinct:

$$G = \sum_i^l G_i$$

Note that the number of subgraphs is upper bounded by the maximum node connectivity of the graph G . That is, if every vertex in G is connected to at most L other vertices, then it is possible to express G as a sum of at most $2L$ subgraphs. Hence, we have the following corollary.

Corollary 10.1.1. *If a graph G has maximum connectivity L , then:*

1. *The squared norm of the signal $E||u||^2$ is d .*
2. *The squared norm of the noise $E||\sum_{i=1}^k s_i||^2$ is $4L^2kd$*
3. *The signal-to-noise ratio is $\frac{1}{4L^2kd}$*

Note that this is a very loose result, since we count each of the k edges L times.

10.2.2 Statistical Error

Now, at this point our query function returns a superposition of the answer u with a noise term $\sum_{i=1}^k s_i$. Hence, we would like to perform a look-up operation to recover u by seeing which of the vertex embeddings the output $u + \sum_{i=1}^k s_i$ is most similar to. In this case, we will use the dot product to measure similarity. Due to the noise term, we might be concerned with the possibilities of recovering the wrong vertex. In particular, Theorem 10.2 suggests that as the number of edges increases, the probability of recovering an incorrect edge increases.

First, consider the dot product of the true answer u with the output:

$$T = \langle u, u + \sum_{i=1}^k s_i \rangle = d + \sum_{i=1}^k \langle u, s_i \rangle = d + \epsilon$$

Thus, the dot product of the true answer T will have $ET = d$ and $Var(T) = kd$. The noise term ϵ is a sum of kd Rademacher random variables, and so $\frac{\epsilon + kd}{2} \sim \text{Binom}(kd, \frac{1}{2})$. The variance of ϵ is kd , and using the normal approximation to the binomial it is of order \sqrt{kd} with high probability. Similarly, consider the dot product of a false vertex v (that does not equal s_i or u) with the output:

$$F = \langle v, u + \sum_{i=1}^k s_i \rangle = \langle v, u \rangle + \sum_{i=1}^k \langle u, s_i \rangle$$

Here, F is the sum of $(k+1)d$ Rademacher random variables, with mean 0 and variance $(k+1)d$; moreover, F is of order $\sqrt{(k+1)d}$ with high probability.

Now, we first approximate the probability that F exceeds $d = ET$. We will use the CLT/Gaussian approximation to Binomial to approximate the sum of n iid Rademachers X as $N(0, n)$. Then, we can use these Gaussian bounds:

$$\frac{C}{t} e^{-\frac{t^2}{2}} \leq P(X > t\sqrt{n}) \leq C e^{-\frac{t^2}{2}}$$

where C is some constant. Hence, applying this to F :

$$C \sqrt{\frac{(k+1)}{d}} e^{-\frac{d}{2(k+1)}} \leq P(F > d) = P(F > \sqrt{\frac{d}{(k+1)}} \sqrt{(k+1)d}) \leq e^{-\frac{d}{2(k+1)}}$$

Thus, this suggests the limit of edges we can store in superposition and still have accurate recovery is $O(d)$. A similar computation shows the probability of T being less than 0 scales in a similar manner:

$$C \sqrt{\frac{k}{d}} e^{-\frac{d}{2k}} \leq P(T < 0) \leq e^{-\frac{d}{2k}}$$

In fact, we can be a bit more precise and compute a lower bound on the probability of correct recovery.

Theorem 10.2. *Under the above setup, let A be the correct recovery event given M erroneous choices: the event where the correct vertex u is most similar to the output of the edge query relative to M other wrong candidate vertices. Then, for some constant C we have:*

$$P(A) \geq 1 - M e^{-\frac{d}{2(2k+1)}}$$

Proof. Now, let us first compute the lower bound. Note that correct recovery is precisely the event where the similarity of the correct vertex $T = \langle u, u \rangle$ is larger

than the similarities $F_1 \dots, F_M$ of the M erroneous vertices, where $F_i = \langle v_i, u \rangle$ for the erroneous vertex v_i . Then,

$$P(T > \max(F_1, \dots, F_M)) = P(\cap\{T > F_i\}) = 1 - P(\cup\{T \leq F_i\})$$

By construction, the F_i 's are iid. Letting ϵ denote the error term:

$$\begin{aligned} P(\cup\{T \leq F_i\}) &\leq \sum_{i=1}^M P(T \leq F_i) \\ &= MP(T \leq F_1) \\ &= MP(d + \epsilon \leq F_1) \\ &= MP(F_1 - \epsilon \geq d) \\ &\leq Me^{-\frac{d}{2(2k+1)}} \end{aligned}$$

Hence

$$P(T > \max(F_1, \dots, F_M)) \geq 1 - Me^{-\frac{d}{2(2k+1)}}$$

We used the fact that a difference of Rademacher sums is still a Rademacher sum, so $F_1 - \epsilon$ is a sum of $(k+1)d + kd = (2k+1)d$ Rademachers. \square

This theorem confirms the informal analysis of this section: the number of edges k that be stored in superposition cannot be more than $O(d)$ without seriously compromising the accuracy of the edge query.

10.3 Hadamard Product and Continuous Codes

Now, let us suppose the we were working with any continuous code (Gaussian, Cauchy, Uniform). Our edge query would now be unbinding the graph by the reciprocal of the query vertex u :

$$Q(u, G) = u^{-1} \odot (u \odot v + \sum_{i=1}^k q_i \odot s_i) = v + \sum_{i=1}^k u^{-1} \odot q_i \odot s_i$$

In the noise term, note that we now have a sum of vector whose entries are ratios: $\frac{q_i}{u^{-1}} s_i$. In section 9, we saw that the entries will have undefined moments: they follow heavy-tailed distribution. Thus, it is very likely that the noise overwhelms the true answer v regardless of how many edges k are in superposition. This makes such continuous codes infeasible for vertex queries.

10.4 Tensor Product and Spherical Codes

Here, we look at the same error quantities for the tensor-spherical scheme: the error norms and the probability of retrieving the correct vertex.

10.4.1 Error Norms

Now, our edge query is of the form:

$$Q(v, G) = v^T(vu^T + \sum_{i=1}^k q_i r_i^T) = u^T + \sum_{i=1}^k \langle v, q_i \rangle r_i^T = u^T + \sum_{i=1}^k s_i^T$$

We have a corresponding result on the average squared norms and the signal-to-noise ratio.

Theorem 10.3 (Tensor-Spherical Signal-to-Noise). *When performing a edge query with a single correct vertex u , under the tensor product and spherical codes of dimension d we have:*

1. *The squared norm of the signal $E||u||^2$ is 1.*
2. *The squared norm of the noise $E||\sum_{i=1}^k s_i||^2$ is $\frac{k}{d}$*
3. *The signal-to-noise ratio is $\frac{d}{k}$*

Proof. The first claim holds since spherical codes have norm 1. The squared norm of the nuisance term $\sum_{i=1}^k \langle v, q_i \rangle s_i^T$ is:

$$E||\sum_{i=1}^k \langle v, q_i \rangle s_i^T||^2 = \sum_i E(\langle v, q_i \rangle)^2 + 2 \sum_{j \neq k} E\langle v, r_j \rangle \langle v, r_k \rangle \langle r_j, r_k \rangle = \frac{k}{d}$$

Hence, the ratio of the answer-noise average norms is $\frac{d}{k}$

□

10.4.2 Statistical Error

Now, we again want to recover the answer u by finding which vertex embedding the query output is most similar to, and we will again use the dot product to measure similarity. First, the dot product of the true answer u with the query output:

$$T = u^T(u + \sum_{i=1}^k \langle v, q_i \rangle r_i) = 1 + \sum_{i=1}^k \langle v, q_i \rangle \langle u, r_i \rangle = 1 + \epsilon$$

The noise term ϵ is a sum of k terms of the form $e_i = \langle v, q_i \rangle \langle u, r_i \rangle$, and using independence and the Cauchy-Schwarz inequality:

$$Ee_i = 0 \quad ; \quad Ee_i^2 = \frac{1}{d^2} \quad ; \quad E|e_i| \leq \frac{1}{d}$$

Hence, the variance of ϵ is $\frac{k}{d^2}$, and so for accurate retrieval we see that $k \leq O(d^2)$ or else ϵ will be of the same magnitude as the signal 1. Similarly, the dot product of a false vertex t (not matching any of the v_i 's) is:

$$F = \langle t, u \rangle + \sum_{i=1}^k \langle v, q_i \rangle \langle t, r_i \rangle = \langle t, u \rangle + \epsilon$$

We first calculate the probability that F exceeds the $ET = 1$. However, since F is sum of random variables with a different distribution, so we make one further simplification. As in section 9.1, the term $\langle t, u \rangle$ will be of the order $\frac{1}{\sqrt{d}}$ with high probability. In fact, using Bernstein's inequality gives:

$$P(|\langle t, u \rangle| > \frac{C}{\sqrt{d}}) \leq e^{-\frac{C^2}{d}/(\frac{1}{d} + \frac{C}{\sqrt{d}})} \leq \exp\{-C^2\}$$

Hence, we assume that $|\langle t, u \rangle| = O(\frac{1}{\sqrt{d}})$, and for large d we can make the following simplification:

$$P(F > 1) \lesssim P(\epsilon > 1 - O(\frac{1}{\sqrt{d}})) \approx P(\epsilon > 1)$$

Hence, as $\epsilon = \sum^k e_i$ where e_i 's are independent with $Ee_i^2 = \frac{1}{d^2}$, then Bernstein's inequality gives:

$$P(F > 1) \approx P(\epsilon > 1) \leq e^{-1/[2(\frac{k}{d^2} + \frac{1}{3})]} \approx e^{-\frac{d^2}{2k}}$$

A similar computation. using the fact that ϵ is symmetrically distributed, gives an upper bound of $e^{-\frac{d^2}{k}}$ for $P(T < 0)$. Hence, both suggest that the limit of edges we can store in superposition and still have accurate recovery is $O(d^2)$.

As in the Hadamard-Rademacher case, we have corresponding bound on the probability of accurate recovery for the tensor-spherical scheme.

Theorem 10.4. *Under the Hadamard-Rademacher scheme, let A be the correct recovery event given M erroneous choices: the event where the correct vertex u is most similar to the output of the edge query relative to M other wrong candidate vertices. Then, for some constant C we have:*

$$P(A) \gtrsim 1 - Me^{-\frac{d^2}{k}}$$

We use the approximation \gtrsim because we condition on the event that the mismatch term $|\langle t, u \rangle| \leq \frac{C}{\sqrt{d}}$, which is true with probability at least $1 - e^{-C^2}$.

Proof. First, we compute the lower bound.. We have:

$$P(T > \max(F_1, \dots, F_M)) = 1 - P(\cup\{T \leq F_i\})$$

We can make the same simplifying conservative assumption of $|\langle t, u \rangle| = O(\frac{1}{\sqrt{d}})$ as above to get:

$$\begin{aligned}
P(\cup T \leq F_i) &\leq \sum P(T \leq F_i) \\
&= MP(T \leq F_1) \\
&= MP(1 + \epsilon_1 \leq \langle t, u \rangle + \epsilon_2) \\
&\lesssim MP(\epsilon_2 - \epsilon_1 \geq 1 + O(\frac{1}{\sqrt{d}})) \\
&\leq Me^{-\frac{d^2}{k}}
\end{aligned}$$

Thus,

$$P(T > \max(F_1, \dots, F_M)) \gtrsim 1 - Me^{-\frac{d^2}{k}}$$

□

Thus, this also confirms that when the vertex code dimension is d , we cannot store more than d^2 edges using the tensor-spherical scheme without compromising the accuracy of the edge query.

10.5 Memory and Capacity

As a reminder, the vertex code has dimension d . Then, using the Hadamard product with Rademacher codes, the graph embedding space is also dimension d ; the previous analysis suggests that we can store at most $k = O(d)$ edges in superposition without seriously affecting the accurate retrieval of the answer. On the other hand, using the tensor product with spherical codes, the graph embedding space is d^2 , and the previous analysis shows that we can store at most $k = O(d^2)$ edge without affecting accuracy. Hence, in both cases the number of edges we can store in superposition vs. the dimension of the graph embedding space have the same ratio.

11 Binding Comparison: Edge Composition

In this section, we focus on the accuracy of edge composition. We are given a graph that contains two composable edges (u, v) and (v, w) , with all other edges having disjoint vertices. Edge composition should return only the valid edge (u, w) , and we perform a edge query checking if the embedding contains (u, w) . The analysis of this section follows the same procedure as the previous section, analyzing the memory and capacity of the tensor-spherical and Hadamard-Rademacher schemes.

11.1 Overview

We work with the following fixed graph:

$$G = \psi(u, v) + \psi(v, w) + \sum_{i=1}^{k-1} \psi(q_i, r_i)$$

where all the q, r 's are distinct from u, v, w and ψ denotes the binding operation. We will look at edge composition, checking specifically for the correct composition of the two composable edges:

$$(u, v) \circ (v, w) \mapsto (u, w)$$

To check for the presence of the correct edge, we will perform an edge query and analyze both the error norms and probability of successfully retrieving the correct edge.

11.2 Hadamard Product and Rademacher Codes

11.2.1 Error Norms

We want to do edge composition with G , which in this case represents just the binding of G with itself:

$$G \odot G = (u \odot v + v \odot w + \sum_{i=1}^{k-1} q_i \odot r_i) \odot (u \odot v + v \odot w + \sum_{i=1}^{k-1} q_i \odot r_i)$$

After distributing, we will get $(k+1)^2$ total terms:

$$G \odot G = u \odot w + \sum_{i=1}^{(k+1)^2-1} e_i = u \odot w + R$$

We assumed that all every vertex was distinct, so each e_i is a Hadamard product of either two or three vertices. Since a product of Rademachers is still Rademacher, each e_i is a Rademacher vector and ϵ is a sum of $(k+1)^2 - 1 = k^2 + 2k$ independent Rademacher vectors.

Theorem 11.1 (Hadamard-Rademacher Signal-to-Noise). *When performing a edge query with a single correct edge (u, v) , under the Hadamard product and Rademacher codes of dimension d we have:*

1. *The squared norm of the signal $E||u \odot w||^2$ is d .*
2. *The squared norm of the noise $E||R||^2$ is $(k^2 + 2k)d$*

3. The signal-to-noise ratio is $\frac{1}{k^2}$

Proof. By construction there is only one correct composable edge in $G - u \odot w$ - and all other terms are noise. Using the results from section 9.2, we can characterize the signal-to-noise ratio.

$$E||u \odot w||^2 = d \quad E||R|| = \sum_i E||e_i||^2 + \sum_{j \neq k} E\langle e_j, e_k \rangle = (k^2 + 2k)d$$

□

11.2.2 Statistical Error

After performing edge composition, we have a superposition of the single composed edge in $G - u \odot w$ - along with noise ϵ . Now, say we want to recover exactly which edges were composable in G . To this end, we can do two things: we can either unbind by one vertex and compute a dot product with the other, or we can unbind by the given edge and then sum all the entries together. Both approaches give the same result, so we shall focus on the latter for simplicity.

Hence, we shall detect the (non)existence of a candidate edge $s \odot t$ by first unbinding and then summing the entries:

$$G \odot G \mapsto (s \odot t) \odot (G \odot G) \mapsto \text{sum}[(s \odot t) \odot (G \odot G)]$$

Now, let us first consider checking the true edge $u \odot w$:

$$(u \odot w) \odot (u \odot w + E) = (1 + E')$$

Unbinding by the true edge will generate a vector of 1's and, as a product of Rademachers is still Rademacher, a new error term ϵ' that, like ϵ , is a sum of $k^2 + k$ independent Rademacher vectors. Now, we then sum up the entries (or equivalently compute the dot product with the vectors of 1's) and we get:

$$T = \text{sum}(1 + E') = d + \sum_{i=1}^{d(k^2-2k)} r_i = d + \epsilon$$

where each r_i is a Rademacher random variable. Therefore, we use the same arguments as the edge query section to get $E(T) = d$ and $\text{Var}(T) = d(k^2 - 2k)$. The noise term ϵ has variance $d(k^2 - 2k)$, and so it is of order $\sqrt{d(k^2 - 2k)} \approx k\sqrt{d}$. This suggests that for accurate retrieval, the number of edge in superposition $k \leq O(\sqrt{d})$.

Similarly, we now do the same procedure for a false random edge $s \odot t$, and since it does not match then we will get sum of $d(k^2 - 2k + 1)$ Rademachers. Thus, the output F of any false edge is:

$$F = \sum^{d(k+1)^2} r_i$$

We conclude that $EF = 0$ and $Var(EF) = d(k+1)^2$.

Repeating the same analysis as in the edge query section, we get the following bounds on the probability that F exceeds $d = ET$:

$$C\sqrt{\frac{(k+1)^2}{d}}e^{-\frac{d}{2(k+1)^2}} \leq P(F > d) \leq e^{-\frac{d}{2(k+1)^2}}$$

Similarly,

$$C\sqrt{\frac{(k^2 - 2k)}{d}}e^{-\frac{d}{2k}} \leq P(T < 0) \leq e^{-\frac{d}{2(k^2 - 2k)}}$$

Finally, for M false edges we have the following result using the same techniques as in the edge query case:

Theorem 11.2. *Under the Hadamard-Rademacher scheme, let A be the correct recovery event given M erroneous choices: the event where the correct edge $u \odot v$ is most similar to the output of the edge query relative to M other wrong candidate edges. Then, for some constant C we have:*

$$P(A) \geq 1 - Me^{-\frac{d}{4(k+1)^2 - 2}}$$

Thus, these all suggest that for accurate edge composition, the number of edges in superposition can be at most \sqrt{d} .

11.3 Tensor Product and Spherical Codes

11.3.1 Error Norm

Using the tensor product, our graph G is:

$$G = uv^T + vw^T + \sum_{i=1}^{k-1} q_i r_i^T$$

and we do edge composition by a matrix multiplication of the graph embedding:

$$G^2 = uv^T + \sum_{i=1}^{(k+1)^2-1} \langle a_i, b_i \rangle d_i c_i^T = uv^T + R$$

where a, b, c, d are all iid uniform from the d -dimensional hypersphere.

Theorem 11.3 (Tensor-Spherical Signal-to-Noise). *When performing a edge query with a single correct edge (u, v) , under the tensor product and spherical codes of dimension d we have:*

1. *The squared Frobenius norm of the signal $E||uw^T||_F^2$ is 1.*
2. *The squared Frobenius norm of the noise $E||R||_F^2$ is $\frac{k^2-2k}{d}$*
3. *The signal-to-noise ratio is approximately $\frac{d}{k^2}$*

Proof. The signal, as the outer product of two orthonormal vectors, has Frobenius norm 1. Similarly, the nuisance term E has the following expected squared Frobenius norm:

$$||E(R^T R)||_F^2 = \text{tr}[E(R^T R)] = \sum_i E(\langle a_i, b_i \rangle)^2 = \frac{k^2 - 2k}{d}$$

Hence, the ratio of the answer-noise average norms is $\frac{d}{k^2-2k} \approx \frac{d}{k^2}$. \square

11.3.2 Statistical Error

Again, we query the edge composition G^2 for the (non)existence of a candidate edge. In the tensor product case, the natural edge query operation for a query edge (s, t) is:

$$s^T G^2 t$$

Hence, let us first examine the result for the only true edge (u, w) :

$$T = u^T (G^2) w = u^T (uw^T + R) w = 1 + u^T R w = 1 + \epsilon$$

Expanding the error term ϵ :

$$\epsilon = u^T R w = u^T \left(\sum_{i=1}^{k^2-2k} \langle a_i, b_i \rangle d_i c_i^T \right) w = \sum_{i=1}^{k^2-2k} \langle a_i, b_i \rangle \langle u, d_i \rangle \langle c_i, w \rangle$$

we see it is a product of $k^2 - 2k$ iid terms, each of which is the product of three independent dot products. Hence, we have $E(\epsilon) = 0$ and $\text{Var}(\epsilon) = \frac{k^2-2k}{d^3} \approx \frac{k^2}{d^3}$, and similarly $ET = 1$ and $\text{Var}(T) = \frac{k^2-2k}{d^3}$. This suggests that $k \leq O(d^{\frac{3}{2}})$ to have accurate edge composition.

Similarly, let us considering querying by any non-existent edge $s \rightarrow t$:

$$F = s^T G^2 t = \langle s, u \rangle \langle w, t \rangle + \sum_{i=1}^{k^2-2k} \langle a_i, b_i \rangle \langle s, d_i \rangle \langle c_i, t \rangle = \langle s, u \rangle \langle w, t \rangle + \epsilon$$

The first term is a product of independent dot products, so it has mean 0 and variance $\frac{1}{d^2}$. The second term has the exact same distribution as the error term in the previous paragraph. We have $EF = 0$ and $Var(F) = \frac{1}{d^2} + \frac{k^2 - 2k}{d^3}$

Now, we first compute the probability that F exceeds $ET = 1$. As in the edge query section, using a Bernstein inequality shows the term $\langle s, u \rangle \langle w, t \rangle$ has magnitude $O(\frac{1}{d})$ with high probability. Hence, we work with the conservative assumption that $|\langle s, u \rangle \langle w, t \rangle| = O(\frac{1}{d})$. For large d we can make the simplification:

$$P(F > 1) \lesssim P(\epsilon > 1 - O(\frac{1}{d})) \approx P(\epsilon > 1)$$

Then, using a Bernstein inequality gives:

$$P(F > 1) \lesssim P(\epsilon > 1) \leq e^{-1/[2(\frac{k^2 + 2k}{d^3} + \frac{1}{3})]} \approx e^{-\frac{d^3}{2k^2}}$$

A similar computation for T , using the fact that ϵ is symmetrically distributed, gives:

$$P(T < 0) \lesssim e^{-\frac{d^3}{2k^2}}$$

These both suggest that we can store at most $O(d^{\frac{3}{2}})$ edges while retaining accurate recovery.

Finally, using the same techniques as that in the edge query section gives us the following result:

Theorem 11.4. *Under the tensor-spherical scheme, let A be the correct recovery event given M erroneous choices: the event where the correct edge uv^T is most similar to the output of the edge query relative to M other wrong candidate edges. Then, for some constant C we have:*

$$P(A) \gtrsim 1 - Me^{-\frac{d^3}{k^2}}$$

We use the approximation \gtrsim because we condition on the event that the mismatch term $|\langle s, u \rangle \langle w, t \rangle| \leq \frac{C}{d}$, which is true with probability at least $1 - e^{-C^2}$.

11.4 Memory and Capacity

The graph embedding dimension under Hadamard product with Rademacher codes is d , and the above analysis gives a limit of \sqrt{d} edges that can be stored in superposition. On the other hand, the tensor product with spherical codes has dimension d^2 and it can store at most $d^{\frac{3}{2}}$ edges in superposition. In both cases, memory-capacity ratio is \sqrt{d} . Again, the Hadamard product with Rademacher codes offers no concrete memory advantages over the tensor product. Any savings we have in memory are offset by a corresponding reduction in capacity.

12 Binding Comparison Summary

From the results of Sections 10 and 11, we see that tensor-spherical and Hadamard-Rademacher embeddings have the same memory-capacity ratio for the edge query and edge composition. We actually do not save any memory by compression via the Hadamard product, since its reduced memory requirement is offset by a proportional penalty on its capacity. Since the circular correlation and convolution are special cases of the Hadamard, this immediately suggests they also suffer the same defect.

12.1 General Memory vs. Capacity Ratio

For both embedding schemes, the edge query is a first-order operation since it can be expressed as a linear operation involving the graph embedding. Similarly, edge composition is a second-order operation since it can be expressed as a multilinear operation, of order 2, involving two copies of the graph embedding. We sketch a general memory-capacity ratio for a n -order operation.

For the Hadamard-Rademacher scheme, a n -order operation on a graph with k edges will create k^n nuisance terms, giving an error term of average squared norm $k^n d$. As we saw in the above sections, we need to scale k such that the variance is at most d^2 . This suggests that at most $d^{\frac{1}{n}}$ edges can be stored in superposition, and the general memory-capacity ratio for the Hadamard-Rademacher scheme is:

$$\frac{d}{d^{1/n}} = d^{1-\frac{1}{n}} = d^{(n-1)/n}$$

For the tensor-spherical scheme an n -order operation will also create k^n edges, but each will be weighted by a random coefficient with mean 0 and variance $d^{-(n+1)}$. During edge recovery, we will then have k^n error terms with mean 0 and variance $d^{-(n+1)}$. From the above section we saw that k needs to scale such that variance is at most 1. This suggests we can store at most $d^{(n+1)/n}$ edges, and the memory-capacity ratio is:

$$\frac{d^2}{d^{(n+1)/n}} = d^{2-(n+1)/n} = d^{(n-1)/n}$$

Therefore, Hadamard-Rademacher embeddings have the same general memory-capacity ratio as the tensor-spherical embeddings, and they offer no real memory advantage.

12.2 Tensor Product and Other Binding Operations

As mentioned in Section 8, the circular correlation and convolution are special cases of the Hadamard product, and the conclusions drawn here for the Hadamard product can be extended to them. While our analysis covers only the Hadamard product paired with Rademacher codes, we note two fundamental defects with the Hadamard product and its related embeddings. Firstly, as we saw in Section 8 the Hadamard product sacrifices some expressivity, where it cannot represent directed edges and edge composition at the same time. Secondly, as we saw in Section 11 the Hadamard product doesn't leverage pseudo-orthogonality to zero out nuisance terms, which partially explains why its memory-capacity ratio matches that of the tensor product; we shall expand on this in the next subsection.

Conversely, two defects of the tensor product are that its dimension explodes with both the binding order and dimension of the original code. In the context of graph embeddings, the first defect is not a concern because the binding order is always small: two for simple graphs or three for typed graphs such as knowledge graphs. The memory-capacity analysis of the previous sections showed the second defect is not a concern relative to other compressed binding operations. Neither defect applies to the tensor product in the context of graph embeddings, and we showed that it is the most expressive and general binding operation.

12.3 Tensor Product and Approximate Orthonormality

From our analyses, we used the approximate orthonormality of spherical codes to control the build-up of error terms when performing graph operations. This property is not unique to spherical codes, and we could achieve similar results with any other pseudo-orthonormal random code. For example, normalized Rademacher codes are another case of a pseudo-orthonormal code.

Theorem 12.1. *Let r_1, \dots, r_k be d -dimensional Rademacher vectors, whose entries are iid Rademacher random variables. Let x_1, \dots, x_k be their normalized versions (ie. $x_i = \frac{1}{\sqrt{d}}r_i$) and let $Z = \langle x_i, x_j \rangle$ denote their dot product for $i \neq j$. The following properties hold:*

1. $\frac{d(Z+1)}{2} \sim \text{Binomial}(d, \frac{1}{2})$.
2. $E(Z) = 0$ and $\text{Var}(Z) = \frac{1}{d}$
3. $P(\max_{i \neq j} |\langle x_i, x_j \rangle| > \epsilon) \geq 1 - 2\binom{k}{2}e^{-\frac{d}{2}\epsilon^2}$

Proof. The first two statements follow from Theorem 9.2, while the third follows by the same argument as in Theorem 7.3. \square

The second derivation in Section 6 suggests that the tensor product leverages pseudo-orthogonality uniquely well, and we compare the tensor and Hadamard products when paired with NR (normalized Rademacher) codes. Consider a graph G consisting of two edges (u, v) and (s, t) . For tensor-NR embeddings, we check if G contains the edge (u, v) through an edge query:

$$u^T(uv^T + st^T)v = 1 + (\langle u, s \rangle)(\langle t, v \rangle)$$

The error term consists of dot products between two pairs of mismatched vertices, and their pseudo-orthonormality shrinks the error term to be of magnitude $\frac{1}{d}$ with high probability. Mismatched vertices interact destructively, and the tensor product uses the pseudo-orthogonality of NR codes to clean up error terms.

On the other hand, consider the same edge query for Hadamard-NR embeddings:

$$\frac{1}{d^2} \text{sum}[(u \odot v) \odot (u \odot v + s \odot t)] = \frac{1}{d^2} \text{sum}[\mathbf{1} + u \odot v \odot s \odot t] = \frac{1}{d^2} (d + \sum_{i=1}^d r_i)$$

Ignoring the common scaling factor of $\frac{1}{d^2}$, the error term is the sum of d Rademacher random variables. Importantly, even though NR codes are pseudo-orthonormal, there is no destructive interaction in the mismatch terms. Although both embeddings use the same vertex code, we see the tensor product leverages orthogonality to control the build-up of error terms, while the Hadamard product does not leverage orthogonality at all.

13 Relationship to Adjacency Matrices

All of the graph operations covered in Section 5 are reminiscent of operations one can do with adjacency matrices. In fact, in the case of exact orthonormal vertex codes our method is a generalization of adjacency matrices. Given a vertex set \mathbf{V} , suppose we encoded each vertex as a unique coordinate vector e_i . Then, for any graph G in \mathbf{V} , its graph embedding would be its adjacency matrix. Moreover, given an orthonormal code $\{v_i\}$, there is always an orthogonal change of basis, represented by orthogonal matrix P , such that:

$$\{v_1, \dots, v_n\} = P\{e_1, \dots, e_n\}$$

Therefore, if A is the adjacency of graph G we have the following relationship to its graph embeddings:

$$G = PAP^T$$

In the exact orthonormal case, our graph embedding is equal to the adjacency matrix up to an orthogonal change of basis. This partly explains their rich representational capacity, since they are capable of any graph operation adjacency matrices can do.

13.1 Generalizing Spectral Machinery

Using exact orthonormal codes, tensor-spherical embeddings are equal to adjacency matrices, up to a change of basis. Immediately, they share any basis-independent property of adjacency matrices, including the spectrum and its related machinery. Given a vector space W and a orthogonal basis B , we can define the generalized diagonal operator on $W \otimes W$ as the operator that only preserves the self-similar tensors:

$$Diag_B : W \otimes W \rightarrow W \otimes W \quad ; \quad b_i \otimes b_j \mapsto \begin{cases} b_i \otimes b_i & i = j \\ 0 & i \neq j \end{cases}$$

Recall that the graph Laplacian L for a graph G with adjacency matrix A and its corresponding diagonal matrix D , defined as:

$$L = D - A$$

Then, using our generalized diagonalization procedure, we can compute generalized graph Laplacian $L(G)$ of our graph embedding G :

$$L(G) = Diag_B(G) - G$$

where $Diag_B$ is the diagonalization operator with respect to our orthogonal basis B . Given two orthogonal bases B_1, B_2 linked by an orthogonal change of basis matrix P , the induced change of basis in the tensor product (in coordinates) would be:

$$e_i e_j^T \mapsto P e_i e_j^T P^T$$

Hence, a diagonalized tensor in the new basis can be expressed as:

$$Diag_{B_1}(\sum_{i,j} a_{ij} e_i e_j^T) = \sum_i a_{ii} e_i e_i^T \mapsto \sum_i a_{ii} (P e_i)(P e_i)^T = P \sum_i (a_{ii} e_i e_i^T) P^T$$

Applying this to our generalized graph Laplacian $L(G)$ gives:

$$L(G) = Diag_V(G) - G = P D P^T - P A P^T = P(D - A)P^T = P L P^T$$

Our generalized graph Laplacian is in fact the usual graph Laplacian, up to an orthogonal change of basis. It has the same spectrum as the usual Laplacian, and

its eigenspaces are related by a distance-preserving transformation. We note that the graph Laplacian of a graph embedding might be expensive to compute, as we shall see in the next section when computing the diagonal term for tensor-spherical embeddings. Instead, we can perform the appropriate change of basis to convert our graph embedding into an adjacency matrix before computing its Laplacian, where diagonalization just requires us to copy the diagonal entries.

If we drop the assumption of an exact orthonormal code and instead use a pseudo-orthonormal code, the only difference is finding an appropriate analogue to the diagonalization operator. Since we will have many more codes than dimensions, we cannot use the change-of-basis trick mentioned above and instead must resort to a more intensive computation. For any vertex code v , let $P_v = vv^T$ denote its associated projection matrix. Conjugation by P_v has the following property:

$$P_v(uw^T)P_v = \langle v, u \rangle \langle v, w \rangle vv^T = \begin{cases} vv^T & u = w = v \\ \approx 0 & u \neq v \text{ or } w \neq v \end{cases}$$

Hence, for a pseudo-orthonormal code V we have the following diagonalization operator:

$$Diag_V(G) = \sum_{v \in V} P_v G P_v$$

This involves multiple matrix conjugations and can be quite expensive. However, tensor-spherical embeddings are compressed relative to an adjacency matrix, and for sparse matrices computing the spectrum of the approximate Laplacian can be cheaper than computing the spectrum of the exact Laplacian. We will discuss this in the next subsection.

13.2 Compressing Sparse Adjacency Matrices

Our graph embeddings are generalizations of adjacency matrices in the idealized case of exact orthonormal codes. However, in practice we use pseudo-orthonormal codes to greatly reduce the dimension; hence, our method may also be viewed as a way to compress adjacency matrices while still retaining their functionality.

Usually, the dimension of the adjacency matrix grows as d^2 with the size of the vertex set d . For sparse matrices, where the number of edges k is much lower than number of total possible connections d^2 , this is very inefficient from a memory perspective since we are using d^2 parameters to represent $k \ll d^2$ edges. Instead, we may view adjacency matrices as special cases of our graph embeddings, representing a superposition of k edges. In Section 10 we showed our graph embeddings only need to scale with the number of edges k in order to preserve accurate first-order graph operations. Hence, rather than using d^2 parameters to

represent a k -sparse graph, tensor-spherical embeddings use the intuitively correct number of k parameters.

The compression offered by tensor-spherical embeddings not only gives memory savings but can also decrease the computational cost of common graph operations. In the previous subsection we discussed an approximate graph Laplacian for tensor-spherical embeddings of the following form:

$$L(G) = \text{Diag}_V(G) - G \quad ; \quad \text{Diag}_V(G) = \sum_{v \in V} P_v G P_v$$

For a graph with k edges, our graph embeddings need be roughly $\sqrt{k} \times \sqrt{k}$ matrices. The complexity of both matrix multiplication and eigenvalue decomposition for $n \times n$ matrices is $O(n^3)$ [17]. Hence, computing the diagonal term in the Laplacian has complexity $O(dk^{3/2})$, and performing an eigenvalue decomposition has complexity $O(k^{3/2})$. In total, computing the graph Laplacian for a tensor-spherical embedding has complexity $O((d+1)k^{3/2})$. Since $k \propto d$ for sparse matrices, the complexity of the graph Laplacian is approximately $O(d^{5/2})$. In contrast, while the diagonal term is easy to compute for an adjacency matrix, its Laplacian will be a $d \times d$ matrix and finding its eigenvalues will have complexity $O(d^3)$. A similar analysis shows that edge composition and other multiplication procedures are cheaper for tensor-spherical embeddings than adjacency matrices.

13.2.1 Comparison to Other Sparse Representations

Tensor-spherical embeddings need to scale with the number of edges k in order to preserve accurate graph representations. How does this compare to other compressed sparse matrix representations?

First, we introduce several common sparse matrix representations and their memory cost. One intuitive representation is Dictionary of Keys (DoK), where each non-zero entry has its row-column index as a key with its corresponding value. This method scales $O(k)$ since the number of key-value pairs equals the number of non-zero entries. The coordinate list representation is similar to DoK, except we now store 3-tuples $(\text{row}, \text{column}, \text{value})$ for each non-zero entry. Finally, the Compressed Sparse Row (CSR) represents a sparse matrix using three arrays containing the non-zero values, their column indices, and the number of non-zero entries above each row respectively. The first two arrays are of length k , while the third is of length $d+1$ where we have d total vertices. Since $d \propto k$ in a sparse matrix, we see that we also need $O(k)$ parameters. Tensor-spherical embeddings match the memory requirements of these sparse matrix representations.

Now, we analyze the complexity of matrix addition for both methods. For each of the sparse matrix representations discussed, matrix addition is $O(k)$ since we

iterate through each value, check if they have matching indices, and sum their values if they do [5] [17]. Similarly, matrix addition of dense matrices of size n is $O(n)$. Since tensor-spherical embeddings are of size k , their addition also has complexity $O(k)$.

Finally, we analyze the complexity of matrix multiplications for each representation. Consider two sparse $d \times d$ matrices A and B with k_1 and k_2 non-zero entries respectively. The worst-case scenario is when all the non-zero entries are concentrated on a single row and column. This gives an intuitive upper bound of $O(k_1 k_2)$, and this upper bound holds when $d^2 \gg k_1, k_2$ [1]. As for tensor-spherical embeddings, the naive algorithm for the multiplication of two $d \times d$ matrices has complexity $O(d^3)$, while Strassen's algorithm improves this to $O(d^{2.372})$ [5]. In order to retain accuracy for a second-order operation like edge composition and matrix multiplication, we saw in Section 11 that a $d \times d$ tensor-spherical embedding can store at most $d^{3/2}$ edges. Thus, in order to store k edges we need them to be roughly $k^{2/3} \times k^{2/3}$ matrices, so their multiplication would be $O(k^2)$ assuming both embeddings have at most k edges. This matches the complexity of the other representations when $k_1 \propto k_2$.

In both memory cost and complexity of linear algebra operations, tensor-spherical embeddings match those of the considered sparse representations - DoK, coordinate list, and CSR format. However, tensor-spherical embeddings have at least one advantage over these methods. As vector representations, they enjoy all of the hardware and software optimizations developed for linear algebraic operations, including advances in parallel computing. Moreover, there has been extensive research in specialized hardware for hyperdimensional computing [12] [11] [16], which can further augment the computational advantages of vector graph representations.

13.3 Proximity to Adjacency Matrices

In this section, we establish a rough bound on how close our graph embeddings are to adjacency matrices. Let us assume we d -dimensional vertex codes for m vertices $\{v_1, \dots, v_m\}$ where $m \leq d$; moreover, this vertex code is ϵ -orthonormal, which holds with high probability for spherical codes from Theorem 7.3. Then, we see that a graph embedding generated from such a code is close to some adjacency matrix.

Theorem 13.1. *For a d -dimensional, ϵ -orthonormal code $V = \{v_1, \dots, v_m\}$ where $m \leq d$, let G be any graph embedding using V with n distinct edges and A be the corresponding adjacency matrix induced from this vertex ordering. Then,*

there exists an orthogonal matrix P such that:

$$\|G - PAP^T\|_F = \|P^T GP - A\|_F < O(nm\epsilon)$$

Proof. We use the Gram-Schmidt process to compute an orthogonal set of vectors u_i from the vertex code $\{v_i\}$:

$$u_i = v_i - \sum_{j=1}^{i-1} \frac{\langle v_i, u_j \rangle}{\langle u_j, u_j \rangle} u_j = v_i - \sum_{j=1}^{i-1} \langle v_i, \bar{u}_j \rangle \bar{u}_j$$

where \bar{u}_j is the unit-length version of u_j . By ϵ -orthonormality, we know that $|\langle v_i, v_j \rangle| < \epsilon$ for all i, j . We know that $u_1 = \bar{u}_1 = v_1$. Then, for u_2 :

$$1 - \epsilon \leq \|u_2\| = \|v_2 - \langle v_2, \bar{u}_1 \rangle \bar{u}_1\| \leq 1 + \epsilon$$

and

$$\|v_2 - u_2\| = \|\langle v_2, \bar{u}_1 \rangle \bar{u}_1\| < \epsilon$$

Hence,

$$\|v_2 - \bar{u}_2\| \leq \|v_2 - u_2\| + \|u_2 - \bar{u}_2\| \leq 2\epsilon \leq m\epsilon$$

Similarly, for $\|u_3\| = \|v_3 - \langle v_3, \bar{u}_1 \rangle \bar{u}_1 - \langle v_3, \bar{u}_2 \rangle \bar{u}_2\|$, let us unravel the term $\langle v_3, \bar{u}_2 \rangle$:

$$|\langle v_3, u_2 \rangle| = |\langle v_3, v_2 \rangle - \langle v_2, \bar{u}_1 \rangle \langle v_3, \bar{u}_1 \rangle| < \epsilon + \epsilon^2$$

This gives:

$$1 - O(2\epsilon) = 1 - \frac{O(2\epsilon)}{1 - \epsilon} \leq \|u_3\| \leq 1 + \frac{O(2\epsilon)}{1 - \epsilon} = 1 + O(2\epsilon)$$

and so:

$$\|v_3 - \bar{u}_3\| \leq O(3\epsilon) \leq O(m\epsilon)$$

Repeating a similar analysis, we see that for m ϵ -orthogonal codes $\{v_1, \dots, v_m\}$, there exists an orthonormal basis $\{\bar{u}_1, \dots, \bar{u}_m\}$ such that $\|v_i - \bar{u}_i\| < O(m\epsilon)$. Hence, let G_V be any graph embedding using the vertex codes $\{v_i\}$ and G_U be the corresponding matrix derived from swapping v_i with \bar{u}_i . Letting $\delta_i = v_i - \bar{u}_i$,

we compute the distance between the two matrices:

$$\begin{aligned}
\|G_V - G_U\|_F &= \left\| \sum_{k=1}^n v_{i_k} v_{j_k}^T - \bar{u}_{i_k} \bar{u}_{j_k}^T \right\|_F \\
&\leq \sum_{k=1}^n \|v_{i_k} v_{j_k}^T - \bar{u}_{i_k} \bar{u}_{j_k}^T\| \\
&= \sum_{k=1}^n \|v_{i_k} v_{j_k}^T - (v_{i_k} + \delta_{i_k})(v_{j_k} + \delta_{j_k})^T\| \\
&= \sum_{k=1}^n \|v_{i_k} v_{j_k}^T - [v_{i_k} v_{j_k}^T + \delta_{i_k} \delta_{j_k}^T - v_{i_k} \delta_{j_k}^T - \delta_{i_k} v_{j_k}^T]\| \\
&\leq \sum_{k=1}^n \|\delta_{i_k} \delta_{j_k}^T\| + \|v_{i_k} \delta_{j_k}^T\| + \|\delta_{i_k} v_{j_k}^T\| \\
&\leq O(nm\epsilon)
\end{aligned}$$

As G_U is a sum of the outer products between the orthonormal \bar{u}_i , we see that $U^T G_U U$ is an adjacency matrix. Since the Frobenius norm is preserved under orthogonal basis change, we see that G_V is $O(nm\epsilon)$ close to an adjacency matrix with respect to the Frobenius norm. \square

14 Experiments

In this section, we perform several experiments confirming the theoretical results of previous section. Firstly, we validate our claim that the dimension of tensor-spherical embeddings needs to scale with the number of edges k rather than the total number of vertices n to retain accurate graph operations. This supports our earlier claim that tensor-spherical embeddings offer a drastic compression of adjacency matrices. Secondly, we look at the accuracy of the query and edge composition when varying the number of edges, for both the tensor-spherical and Hadamard-Rademacher scheme.

14.1 Effect of Varying Codebook Size

We look at the effect of the number of vertices on the accuracy of a edge query. Specifically, we consider the positive and negative case where the queried edge is present and absent respectively, testing for both correct recovery and false positives. We fix the number of edges at 64 and vary the vertex codebook size from 64 to 2048. The vertex code dimension is 16, meaning our graph embeddings will be 16×16 matrices. Each codebook is generated by independently sampling

uniformly from the 64-dimensional unit hypersphere. A graph is generated by randomly selecting 64 pairs of vertices from the codebook and computing their pairwise tensor product; these are then added together to generate the graph. We then perform an edge query using a separately generated edge, and in the positive case this edge is added to the graph before the edge query. For each codebook size we carry out this procedure 200 times and average the results, which are shown in Figure 1.

The results show that the size of the vertex set has no impact on the accuracy of tensor-spherical embeddings, and intuitively this is a tautological result: the only vertices that matter are the ones that participate in the graph, and increasing the vertex codebook only serves to decrease the chance that a particular vertex participates in multiple edges. Interestingly, our graph embeddings were 16×16 yet were able to accurately store 64 edges in superposition. Assuming each edge involves unique vertices, the corresponding adjacency matrix would need to be a 128×128 matrix - an 64-fold increase in the number of parameters used.

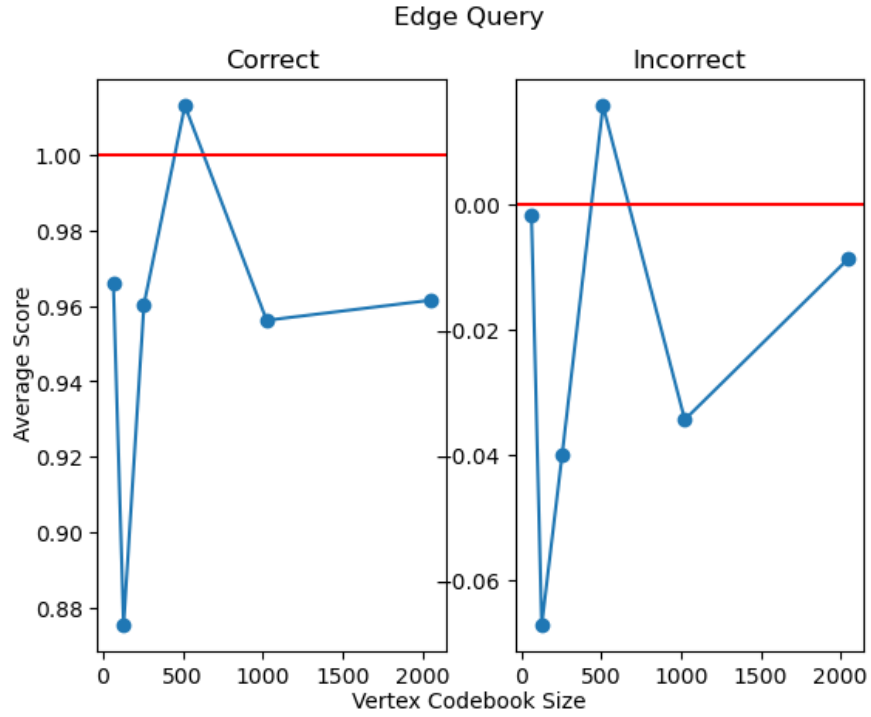


Figure 1: Effect of varying codebook size on edge query performance. Shown above are the average edge query results at each codebook size, averaged over 200 trials. In red are the ideal edge query values for the positive and negative case: 1 in the positive case and 0 in the negative case. Increasing the number of possible vertices does not affect the performance of tensor-spherical embeddings, and in the next experiment we show that accuracy scales with the number of edges.

14.2 Capacity of Graph Embeddings

We also run simulations that confirm our theoretical results on the capacity of tensor-spherical and Hadamard-Rademacher embeddings. For both schemes, we look at their accuracy in the edge query and edge composition. Much like the previous experiment, we had positive and negative versions of each experiment. The procedure is similar to that of the previous section, but now we fix the vertex codebook size to 64 and instead vary the number of edges in superposition from 8 to 500. We set the dimension of the vertex code to 16 for tensor-spherical embeddings and 256 for Hadamard-Rademacher embeddings. This was done so each embedding used the same number of parameters. As a consequence, note that the ideal values for the positive case differ between the two schemes: 1 for tensor-spherical embeddings and 256 for the Hadamard-Rademacher embeddings. For each edge capacity, we performed 200 trials and averaged the results. Figure 2 shows the average results for tensor-spherical embeddings, and Figure 3 shows the average results for Hadamard-Rademacher embeddings. Accounting for the different magnitudes of the ideal values, we see that the accuracy of the two methods scale similarly in both the edge query and edge composition. This supports our theoretical result that the memory vs. capacity ratio is the same for both embeddings.

We note that our theoretical analysis assumed that the graph embeddings had distinct edges, with no repeats. However, in these experiments we generated edges by binding together two vertex codes randomly sampled from a fixed codebook, and it's possible a vertex can participate in multiple edges. We chose this experimental setup because it more closely reflects the conditions of a practical setting. Nonetheless, the empirical results corroborate our theoretical results.

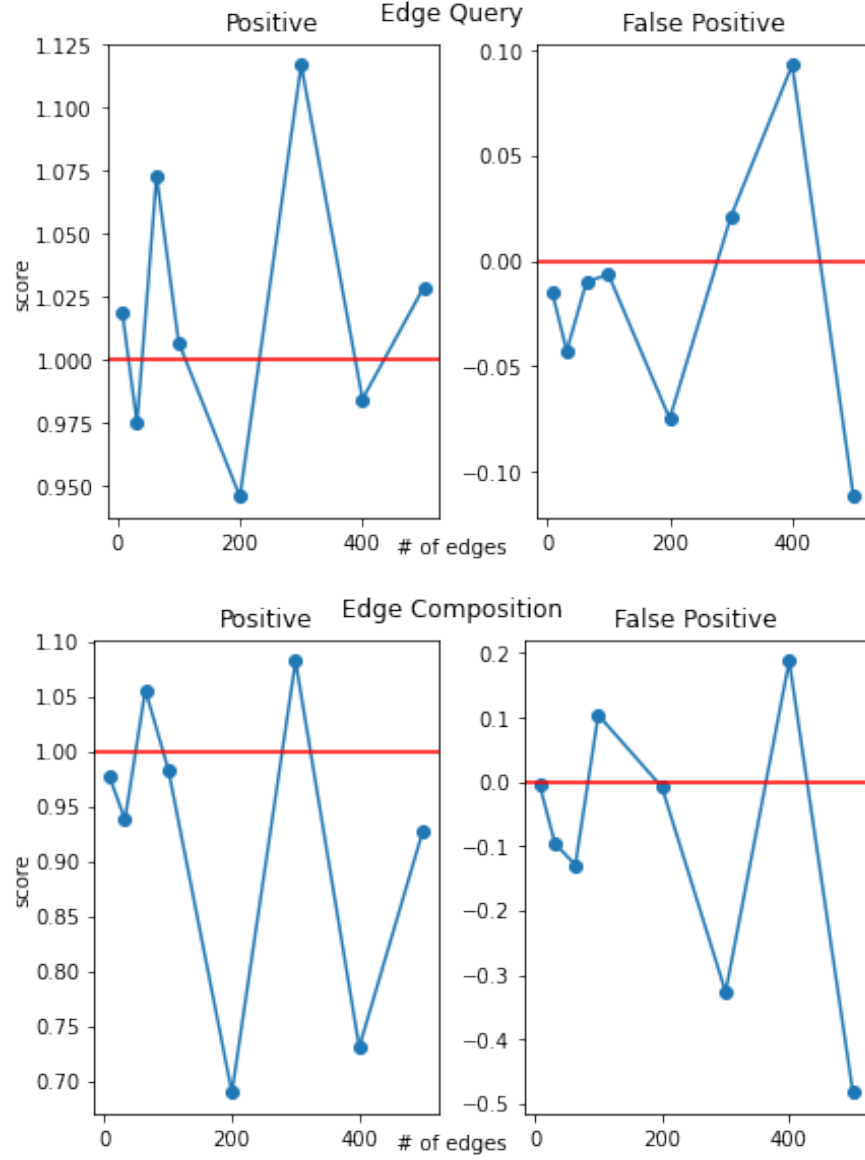


Figure 2: Results for tensor-spherical embeddings. For each edge capacity, we show the average results over 200 trials. The red lines denote the ideal values for the positive and negative cases.

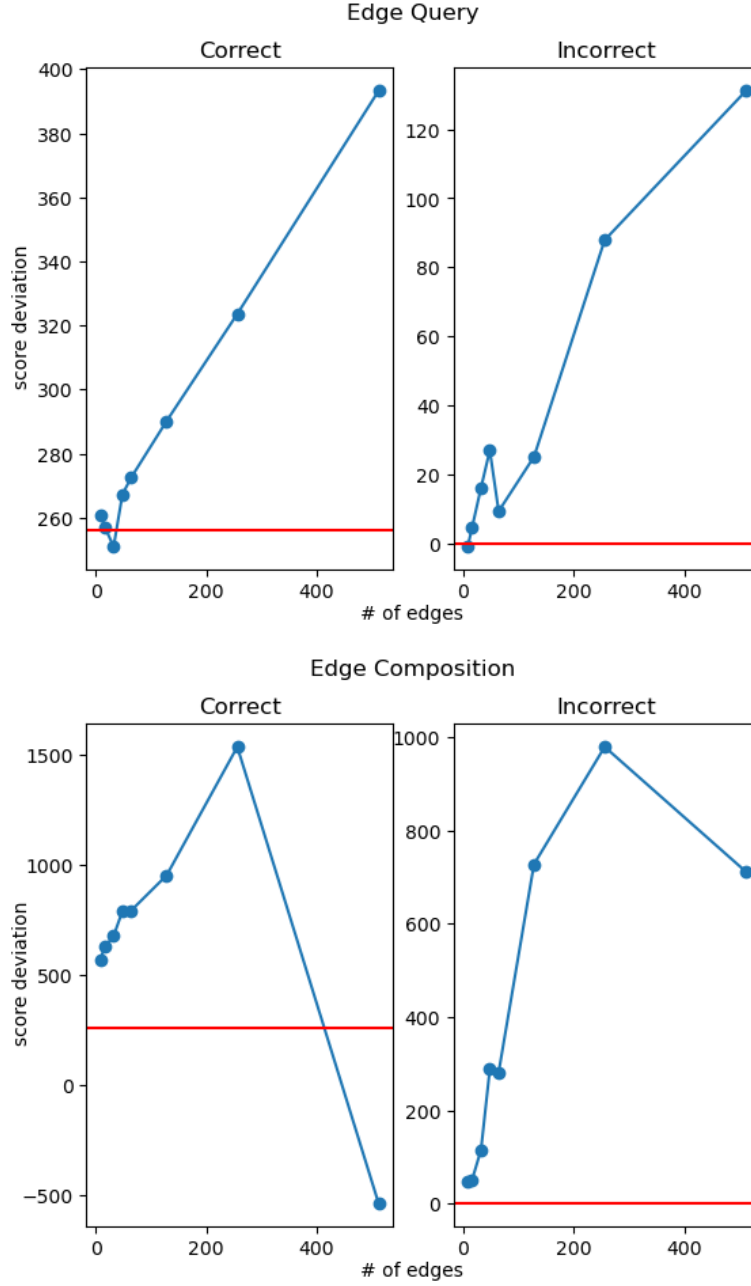


Figure 3: Results for Hadamard-Rademacher embeddings. For each edge capacity, we show the average results over 200 trials. The red lines denote the ideal values for the positive and negative cases.

15 Conclusion

In this paper, we showcased the many nice theoretical properties of tensor-spherical graph embeddings. As compressed generalizations of adjacency matrices, they are capable of a wide range of graph operations while sidestepping the scaling issues that plague adjacency matrices. In particular, we demonstrated their utility in representing sparse matrices, showing they match other sparse matrix representations (dictionary of keys, coordinate list, compressed sparse row) in both parameter usage and complexity of graph operations. Our theoretical and experimental results confirmed that tensor-spherical embeddings can drastically compress adjacency matrices while still retaining accurate graph functionality. The results contained in this paper are incomplete, and the utility of tensor-spherical embeddings as sparse matrix representations is an interesting direction of inquiry.

We also gave several theoretical properties of the tensor product that make it an attractive binding operation for graph embeddings. First, we established a mathematical link between the tensor product and the superposition principle, showing that it's the most general and hence most expressive binding operation among all binding operations that respect superposition. Our analysis also showed that tensor-spherical embeddings have the same memory-capacity ratio as Hadamard-Rademacher embeddings, suggesting the Hadamard product and its derived embeddings (circular correlation and convolution) do not offer any actual memory savings. We demonstrated that this is due in part to the tensor product's ability to leverage pseudo-orthogonality to control error terms, which the Hadamard product lacks. When paired with pseudo-orthonormal codes, the analysis in this paper suggests that the tensor product deserves more attention from the hyperdimensional computing community, at least in the context of graph embeddings.

References

- [1] Keivan Borna and Sohrab Fard. A note on the multiplication of sparse matrices. *Open Computer Science*, 4(1):1–11, 2014.
- [2] Stéphane Boucheron, Gábor Lugosi, and Olivier Bousquet. *Concentration Inequalities*, pages 208–240. Springer Berlin Heidelberg, Berlin, Heidelberg, 2004.
- [3] Brian Cheung, Alex Terekhov, Yubei Chen, Pulkit Agrawal, and Bruno A. Olshausen. Superposition of many models into one. *ArXiv*, abs/1902.05522, 2019.
- [4] Kenneth L. Clarkson, Shashanka Ubaru, and Elizabeth Yang. Capacity analysis of vector symbolic architectures, 2023.
- [5] Thomas H. Cormen, Charles E. Leiserson, Ronald L. Rivest, and Clifford Stein. *Introduction to Algorithms, Third Edition*. The MIT Press, 3rd edition, 2009.
- [6] Ross W. Gayler and Simon D. Levy. A distributed basis for analogical mapping. 2009.
- [7] William B. Johnson and Joram Lindenstrauss. Extensions of lipschitz mappings into a hilbert space. *Contemporary Mathematics*, 26, 1984.
- [8] Pentti Kanerva. *Sparse Distributed Memory*. MIT Press, Cambridge, MA, USA, 1988.
- [9] Jaeyoung Kang, Minxuan Zhou, Abhinav Bhansali, Weihong Xu, Anthony Thomas, and Tajana Rosing. Relhd: A graph-based learning on fefet with hyperdimensional computing. *2022 IEEE 40th International Conference on Computer Design (ICCD)*, pages 553–560, 2022.
- [10] John Kermond. *An Introduction to the Algebra of Random Variables*, pages 1–16. The Mathematical Association of Victoria, 2010.
- [11] Behnam Khaleghi, Sahand Salamat, Anthony Thomas, Fatemeh Asgarinejad, Yeseong Kim, and Tajana Rosing. Shearer: Highly-efficient hyperdimensional computing by software-hardware enabled multifold approximation. In *Proceedings of the ACM/IEEE International Symposium on Low Power Electronics and Design, ISLPED ’20*, page 241–246, New York, NY, USA, 2020. Association for Computing Machinery.
- [12] Denis Kleyko, Mike Davies, E. Paxon Frady, Pentti Kanerva, Spencer J. Kent, Bruno A. Olshausen, Evgeny Osipov, Jan M. Rabaey, Dmitri A. Rachkovskij,

- Abbas Rahimi, and Friedrich T. Sommer. Vector symbolic architectures as a computing framework for nanoscale hardware. In *Proceedings of the IEEE*, volume 10, page 1538–1571, 2022.
- [13] Denis Kleyko, Dmitri A. Rachkovskij, Evgeny Osipov, and Abbas Jawdat Rahim. A survey on hyperdimensional computing aka vector symbolic architectures, part ii: Applications, cognitive models, and challenges. *ArXiv*, abs/2112.15424, 2021.
- [14] Serge Lang. *Algebra*. Springer, New York, NY, 2002.
- [15] Kasper Green Larsen and Jelani Nelson. Optimality of the johnson-lindenstrauss lemma. In *2017 IEEE 58th Annual Symposium on Foundations of Computer Science (FOCS)*, pages 633–638, 2017.
- [16] Haitong Li, Tony F. Wu, Abbas Rahimi, Kai-Shin Li, Miles Rusch, Chang-Hsien Lin, Juo-Luen Hsu, Mohamed M. Sabry, Sukru Burc Eryilmaz, Joon Sohn, Wen-Cheng Chiu, Min-Cheng Chen, Tsung-Ta Wu, Jia-Min Shieh, W. K. Yeh, Jan M. Rabaey, Subhasish Mitra, and H. S. Philip Wong. Hyperdimensional computing with 3d vrram in-memory kernels: Device-architecture co-design for energy-efficient, error-resilient language recognition. *2016 IEEE International Electron Devices Meeting (IEDM)*, pages 16.1.1–16.1.4, 2016.
- [17] Yan Li, Sheng-Long Hu, Jie Wang, and Zheng-Hai Huang. An introduction to the computational complexity of matrix multiplication. *Journal of the Operations Research Society of China*, 8(1):29–43, 2020.
- [18] Yunpu Ma, Marcel Hildebrandt, Volker Tresp, and Stephan Baier. Holistic representations for memorization and inference. In *UAI*, 2018.
- [19] George Marsaglia. Ratios of normal variables and ratios of sums of uniform variables. *Journal of the American Statistical Association*, 60(309):193–204, 1965.
- [20] Maximilian Nickel, Xueyan Jiang, and Volker Tresp. Reducing the rank in relational factorization models by including observable patterns. In Z. Ghahramani, M. Welling, C. Cortes, N. Lawrence, and K.Q. Weinberger, editors, *Advances in Neural Information Processing Systems*, volume 27. Curran Associates, Inc., 2014.
- [21] Maximilian Nickel, Lorenzo Rosasco, and Tomaso A. Poggio. Holographic embeddings of knowledge graphs. In *AAAI*, 2016.
- [22] Maximilian Nickel and Volker Tresp. Logistic tensor factorization for multi-relational data, 2013.

- [23] Igor O. Nunes, Mike Heddes, Tony Givargis, Alexandru Nicolau, and Alexander V. Veidenbaum. Graphhd: Efficient graph classification using hyperdimensional computing. *2022 Design, Automation & Test in Europe Conference & Exhibition (DATE)*, pages 1485–1490, 2022.
- [24] T.A. Plate. Holographic reduced representations. *IEEE Transactions on Neural Networks*, 6(3):623–641, 1995.
- [25] Prathyush Poduval, Haleh Alimohamadi, Ali Zakeri, Farhad Imani, M. Hassan Najafi, Tony Givargis, and Mohsen Imani. Graphd: Graph-based hyperdimensional memorization for brain-like cognitive learning. *Frontiers in Neuroscience*, 16, 2022.
- [26] Kenny Schlegel, Peer Neubert, and Peter Protzel. A comparison of vector symbolic architectures. *Artificial Intelligence Review*, 55(6):4523–4555, dec 2021.
- [27] Paul Smolensky. Tensor product variable binding and the representation of symbolic structures in connectionist systems. *Artificial Intelligence*, 46(1):159–216, 1990.
- [28] Anthony Thomas, Sanjoy Dasgupta, and Tajana Simunic. A theoretical perspective on hyperdimensional computing. *J. Artif. Intell. Res.*, 72:215–249, 2020.
- [29] Unai Zulaika, Aitor Almeida, and Diego López-de Ipiña. Regularized online tensor factorization for sparse knowledge graph embeddings. *Neural Comput. Appl.*, 35(1):787–797, sep 2022.